



# Sesquiterpenoid-rich Java Ginger rhizome extract prompts autophagic cell death in cervical cancer cell SiHa mainly by modulating cellular redox homeostasis

Sonali Nath<sup>1</sup> · Debashis Patra<sup>2</sup> · Anish Nag<sup>3</sup> · Rita Kundu<sup>1</sup>

Received: 23 August 2022 / Accepted: 26 November 2022 / Published online: 14 December 2022  
© King Abdulaziz City for Science and Technology 2022

## Abstract

Java Ginger or *Curcuma zanthorrhiza* Roxb. has long gained focus among tribal people of Java, for its medicinal properties mainly against gynaecological challenges. The present study aims to identify the most potent phytochemical present in the extract and determine primary mode of action accountable for cytotoxic activity of *Curcuma zanthorrhiza* rhizome extract against HPV16-positive SiHa cervical cancer cells. The phytochemically-rich extract of rhizome (CZM) was capable to inhibit proliferation of target cells in a dose-dependent manner with an IC<sub>50</sub> of 150 µg/ml. Dysregulation of intercellular antioxidant defence system resulted to surges in ROS and RNS level, increased calcium concentration and compromised mitochondrial membrane potential. Nucleus got affected, cell cycle dynamics got impaired while clonogenicity and migration ability diminished. Expression of viral oncogenes E7 and E6 decreased significantly. Accumulation of toxic cell metabolite and decrease in level of essential ones continued. Finally, alteration in PI3K/AKT/mTOR signalling route was followed by onset of autophagic cell death concomitant with the upregulated expression of Beclin1, Atg5-12 and LC3II. Curcumin and a novel crystal as well as few phyto-fractions were isolated by column chromatography. Of these, curcumin was found to be most potent in inducing cytotoxicity in SiHa while two other fractions also showed significant activity. Thus, CZM acted against SiHa cells by inducing autophagy that commences in compliance to the changes in PI3K/AKT/mTOR pathway mainly in response to oxidative stress. To the best of our knowledge this is the first report of *Curcuma zanthorrhiza* Roxb. inducing autophagy.

**Keywords** Cancer biology · Cell culture · Flow cytometry · Cytotoxicity · Western blot analysis

## Introduction

According to global cancer statistics, 2020, the estimated numbers of new cases and deaths due to cervical cancer throughout the world have increased to 3.2% and 3.3%, respectively. In India, cervical cancer is ranked as the third most commonly occurring cancer accounting for about

18.3% of new cases in 2020 (Mehrotra and Yadav 2022). Surgeries, radiation therapy and chemotherapy to immunotherapy are used, mostly in combinations, to treat cervical cancer. However, due to intense side effects of these methods such as suppression of bone marrow, gastrointestinal lesions, neurologic dysfunctions, cardiac toxicity and other chronic side effects (such as digestive distress, nausea, vomiting and loss of appetite), there is a need in finding other safer approaches.

One such approach is to use phytoextract or phytochemicals (such as phytosterols, polyphenols and terpenoids) since it is known from various reports that use of such natural products can induce comparatively lesser side effects. *Curcuma zanthorrhiza* originated in Indonesia, more specifically in Java Island, and hence is commonly known as the Java Turmeric or Java Ginger. Among the Javanese people, it is commonly known as 'temulawak' and is considerably used in preparation of 'Jamu'—a widely popular

✉ Rita Kundu  
kundu\_rita@yahoo.co.in

<sup>1</sup> Centre of Advanced Study, Department of Botany, University of Calcutta, 35, Ballygunge Circular Road, Kolkata 700019, India

<sup>2</sup> Department of Chemistry, Taki Government College, Taki 743426, West Bengal, India

<sup>3</sup> Department of Life Sciences, Christ University, Bangalore 560029, Karnataka, India

natural health drink. Indonesian Drug and Food Authority have established the plant as a distinguished therapeutic plant with stellar prospects (Ervintari et al. 2019). Its use in wound healing (Kim et al. 2007) as well as in abrogating inflammation has been extensively recorded in conventional folk medicine (Jantan et al. 2021). Further, such claims have been scientifically established with modern research. In Malaysia, the plant has been long used in domestic treatment of diverse maladies ranging from rheumatism to hepatitis. At certain regions, it is also utilised for curing liver and gastrointestinal ailments (Jantan et al. 2021). In Java, it has risen to prominence as a unique immunity booster and its immunomodulatory capability has been reinforced with exemplary safety profile (Setyati et al. 2019). It is also used as a flavouring as well as colouring spice in traditional delicacies. On the other hand, locals of Javanese community, especially the Enggano, Urug and Madura tribes, further identify this plant with the cure of haemorrhoid, vaginal discharge and other gynaecological disorders (Rahmat et al. 2021). Interestingly, these problems often are associated with prognosis of cervical cancer. *Curcuma zanthorrhiza* Roxb. is rich in flavonoids and harbours xanthorrhizol, a sesquiterpenoid of bisabolane-type that is present in no other species of *Curcuma*, thereby making it unique. In HPV (Human Papillomavirus)-18-positive HeLa cells (human cervical carcinoma), its ethanolic extract caused apoptotic cell death (Ismail et al. 2005). Thus, anticarcinogenic activity of the plant has been inquired only marginally and it has the potential to be a promising candidate to be explored further.

Among the non-apoptotic modes of cell death, autophagy often secures the foremost position. It is an essential eukaryotic degradative process that primarily aids in quality control of organelles and cellular macromolecules. Although this conserved process helps in maintaining homeostasis by recycling important components for ideal functioning of the cell, dysregulation of autophagy has been observed under abnormal physiological conditions. In cancer, it acts dichotomously as in some cases it facilitates tumour progression while in others it assists in overriding the latter. Presently, the modulation of autophagic process in cancer cells under the influence of phytotherapeutic extracts is being extensively evaluated.

In this study, we have observed that methanolic extract of *Curcuma zanthorrhiza* rhizome induces oxidative stress-mediated autophagy that ultimately leads to cell death in cervical cancer cell line SiHa (HPV 16-positive). We have also tried to isolate the most effective bioactive compound from the extract that might be responsible for actuating cell death in SiHa. To the best of our knowledge, this is the first report of *Curcuma zanthorrhiza* inducing autophagic cell death in a cancer cell line.

## Materials and methods

Detailed experimental methods have been provided in supplementary file S1.

### Preparation of plant extract

The rhizomes of *Curcuma zanthorrhiza* Roxb. (reference specimen number CALI122535, present in Calicut University Herbarium) were obtained from garden of Calicut University in the month of October 2017 and were authenticated by Prof. Mamiyil Sabu, Head of the Department of Botany, Calicut University. They were cleaned, cut into fine slices and air-dried in shade to obtain thin flakes. These were then ground to get fine powder of the sample. The dried and powdered sample was extracted in methanol (CZM), ethyl acetate (CZE), petroleum ether (CZP) and distilled water (CZW) individually (2 g of powdered sample in 20 ml of solvent) for 7 days. The respective extracted solutions were then dried/lyophilized for 3 days to obtain the crude test samples and stored at  $-20\text{ }^{\circ}\text{C}$  until further use. For the cytotoxicity tests, the extracts were further dissolved in dimethyl sulfoxide (DMSO) (100 mg/ml) while for the phytochemical assays they were dissolved in respective parent solvents.

### Cell culture

The cell lines SiHa (human cervical cancer) and HEK293 (human embryonic kidney) were obtained from the NCCS, Pune, India. These were maintained in DMEM (HiMedia) supplemented with 10% FBS (HiMedia) and 1% antibiotic-antimycotic solution (HiMedia) inside humidified incubator with 5%  $\text{CO}_2$ .

### Cytotoxicity assay

MTT reduction assay was performed as described by Mosmann 1983. Trypan blue dye exclusion test of cell viability was performed as described by Chiruvella et al. 2010.

### Wound healing assay

Wound healing assay was performed as described by Liang et al. 2007.

### Colony formation assay

Colony forming assay was performed as described by Franken et al. 2006. Approximately 240 cells were seeded in 6-well plate and treated with the CZM for 7 days.

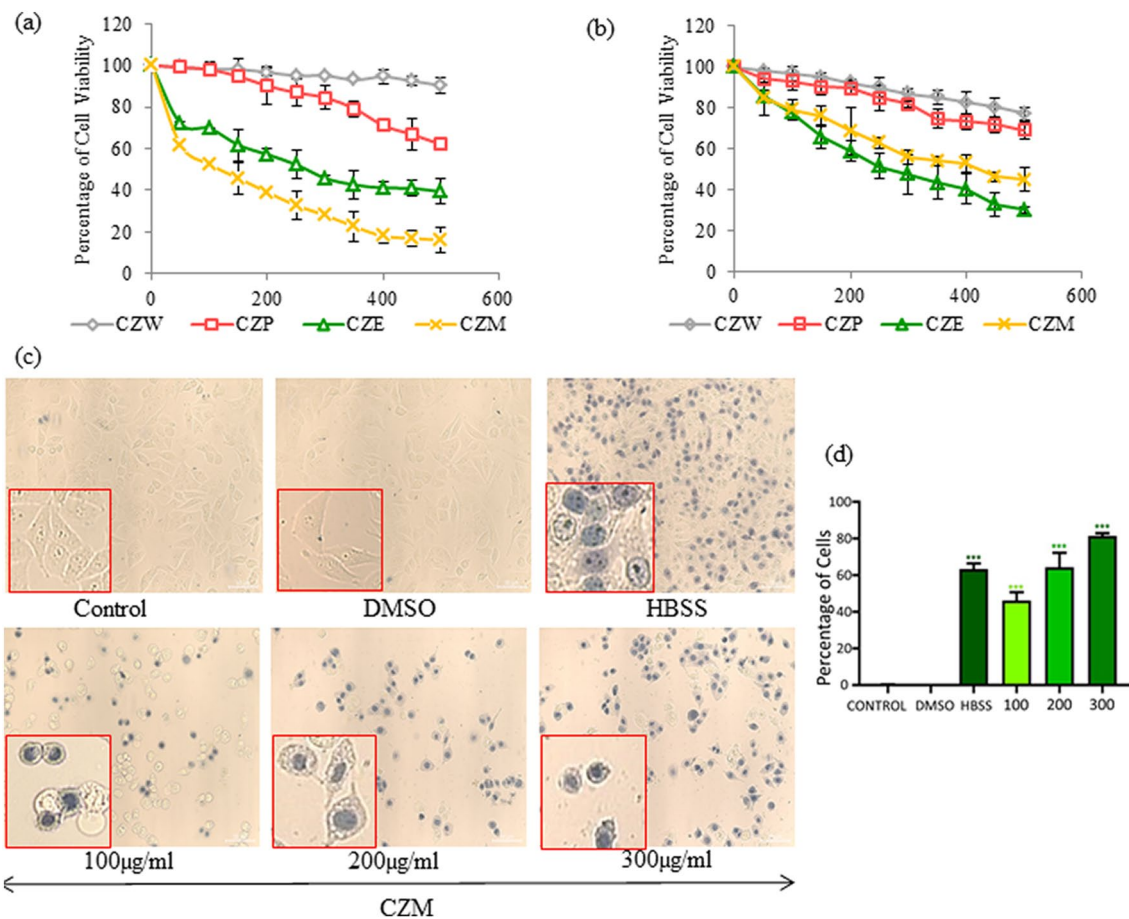


**Fig. 1** CZM exhibited selective cytotoxicity. **a** and **b** Line graphs showing percentage decrease in cell viability in SiHa and HEK293 cells treated with CZ rhizome extracts at 24 h as detected by MTT reduction assay. **c** Microscopic images depicting increase in cytotoxicity of CZM against SiHa following treatment time of 24 h as observed through Trypan blue exclusion assay. Inset images display-

ing zoomed form of affected cells. Effects of DMSO (vehicle control) and HBSS (positive control) on the cells have also been depicted. Scale represents 50  $\mu\text{m}$ . **d** Bar graph showing corresponding dose-dependent increase in percentage of non-viable SiHa cells on treatment with CZM. Data has been presented as mean  $\pm$  SD ( $n=3$ ). \* $P < 0.01$ , \*\* $P < 0.001$ , \*\*\* $P < 0.0001$

### Cell cycle dynamics analysis

Cell cycle dynamics analysis was performed according to Pal et al. 2021.

### Acridine orange assay

Acridine orange assay was performed according to Thomé et al. 2016 and Majumder et al. 2020.

### Monodansylcadaverine assay

Formation of late autophagosomes in the treated cells was detected by flow cytometry (BD FACSVersé, BD Biosciences, USA) using Monodansylcadaverine (0.075 mM, 30 min).

### Cellular and nuclear morphology analysis

Cellular and nuclear morphological changes after 24 h of treatment were detected by Haematoxylin–Eosin (1%) staining method and Hoechst 33,258 (1  $\mu\text{g}/\text{ml}$ ) staining method, respectively. The sets were observed under microscope (Leica, Germany) and photographed.

### Halo assay

Halo assay was performed as described by Sestili et al. 2017.

### Intracellular ROS and NO level analysis

Intracellular ROS and NO level analysis were done according to Wu and Yotnda 2011.

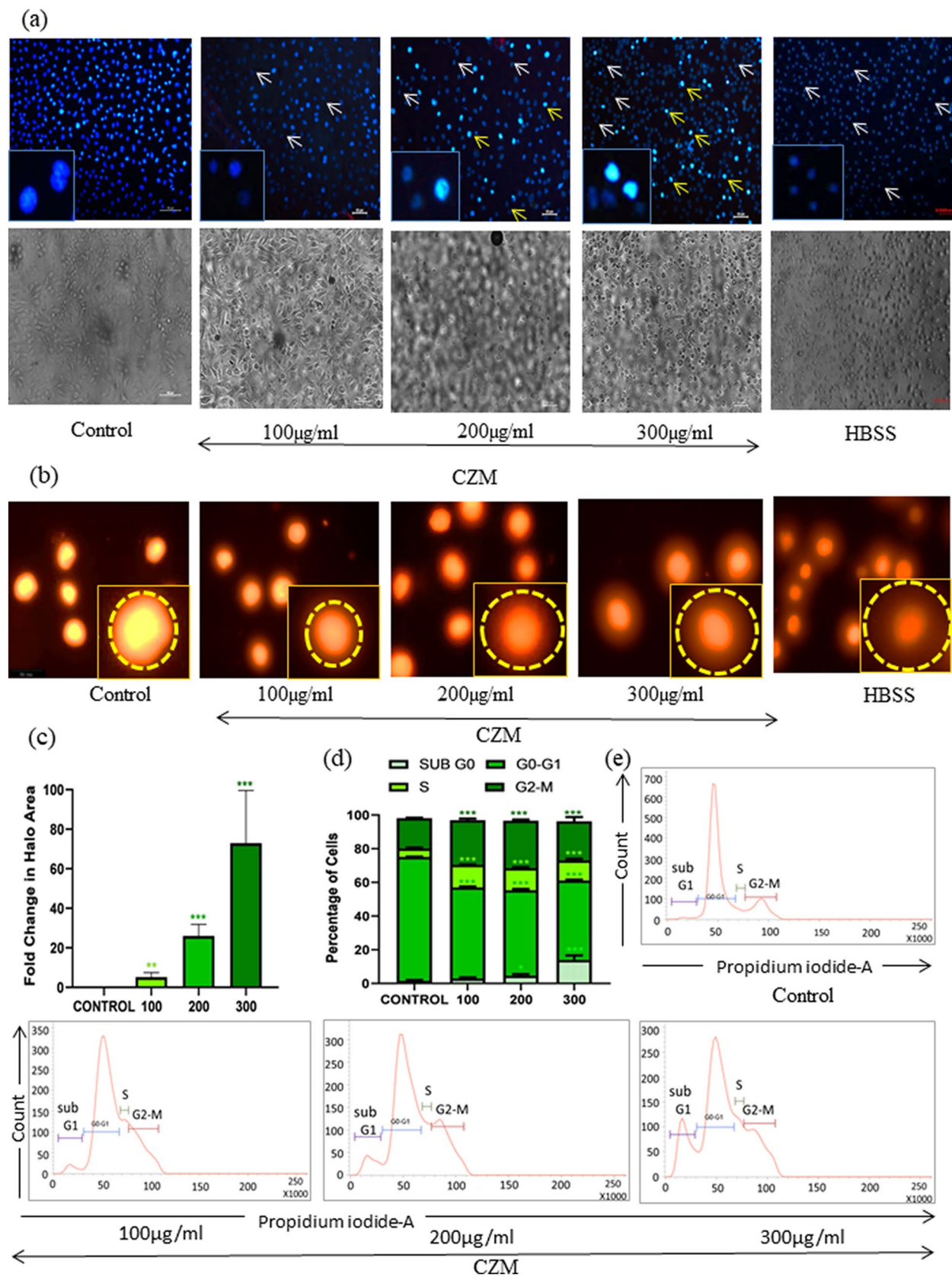


**Fig. 2** CZM inhibited cell proliferation in SiHa. **a** Upper panel showing changes in nuclear morphology of Hoechst 33,342-stained CZM-treated and HBSS-positive SiHa cells through fluorescence microscopy. Lower panel showing corresponding bright-field images. Yellow arrows indicate highly condensed nuclei. White arrows denote nuclei with probable chromosomal erosion. Scale represents 50  $\mu\text{m}$ . **b** Fluorescence microscopy images obtained after subjecting CZM-treated SiHa cells to halo assay indicating incidence of DNA damage. Representative image for each set has been presented inset. Scale represents 20  $\mu\text{m}$ . **c** Bar graphs showing percentage increase in area of halo around nuclei with respect to control set. **d** Bar graphs depicting percentage of cells in each phase. Data has been presented as mean  $\pm$  SD ( $n=3$ ). \* $P < 0.01$ , \*\* $P < 0.001$ , \*\*\* $P < 0.0001$ . **e** Histograms obtained through flow cytometric analysis showing changes in phase distribution of cell cycle in SiHa cells treated with CZM for 24 h

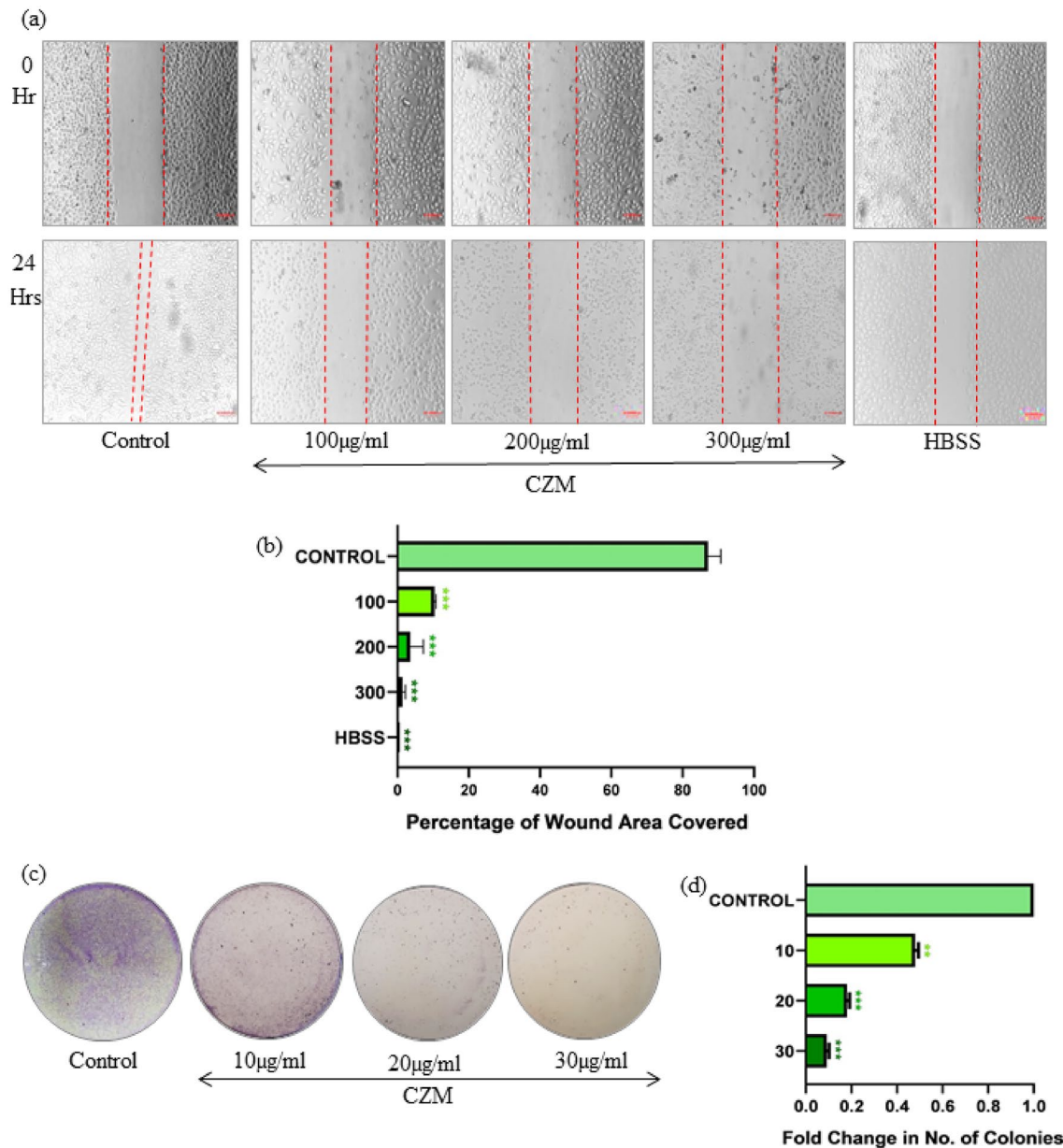


**Fig. 3** CZM prohibited cell migration and clone formation in SiHa. **a** Effect of CZM on cell migration potential of SiHa after 24-h treatment. Upper panel represents scratches photographed immediately after being made. Lower panel represents images taken at 24 h. Dashed red lines indicate area of gap. **b** Bar graph showing corresponding change in cell migration potential in treated cells with

respect to untreated control set. **c** Images of wells showing effect of CZM on clonogenicity of SiHa after a treatment time of 7 days. **d** Bar graph showing corresponding change in clone-formation potential in treated cells with respect to untreated control set. Data has been presented as mean  $\pm$  SD ( $n=3$ ). \* $P < 0.01$ , \*\* $P < 0.001$ , \*\*\* $P < 0.0001$

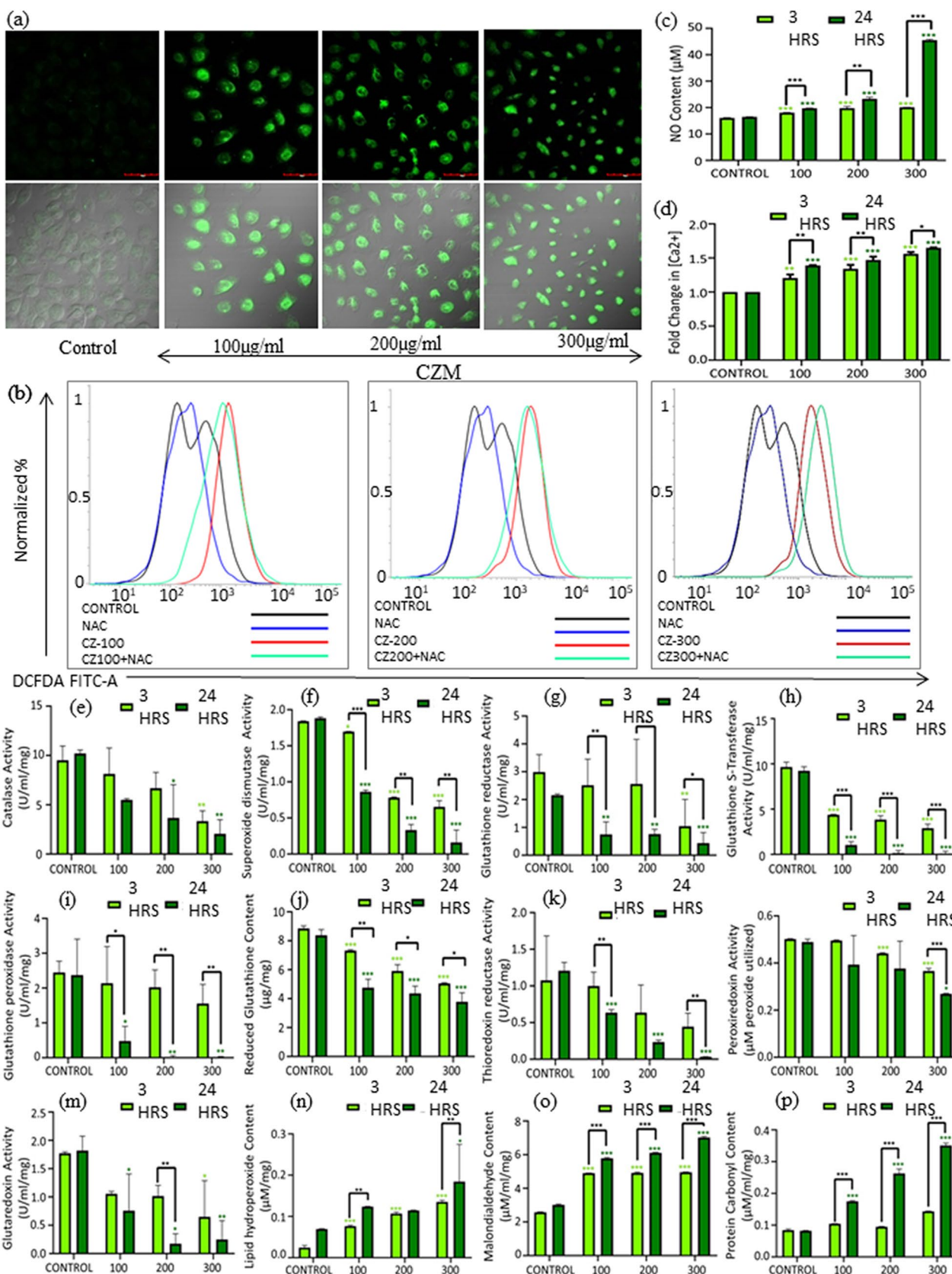


**Fig. 4** CZM enhanced oxidative stress in SiHa. **a** Upper panel showing confocal microscopy images of DCFDA-stained SiHa cells treated with CZM for 3 h. Lower panel showing corresponding phase contrast images. Scale represents 50  $\mu\text{m}$ . **b** Overlay histograms depicting dose-dependent rise in intracellular ROS in CZM-treated cells as detected from flow cytometric analysis. Effects of pre-treatment with NAC (0.5 mM, 30 min) on ROS generation in all the sets have also been presented in the same. **c** and **d** represent estimated NO content and intracellular calcium ion concentration in CZM-treated SiHa cells at two time points of 3 h and 24 h. **e** Catalase activity in CZM-treated SiHa cells estimated by spectrophotometric assay. **f** Superoxide dismutase activity. **g** Glutathione reductase activity. **h** Glutathione transferase activity. **i** Glutathione peroxidase activity. **j** Reduced glutathione content. **k** Thioredoxin reductase activity. **l** Peroxiredoxin activity. **m** Glutaredoxin activity. **n**, **o** and **p** represent, respectively, the estimated contents of the oxidative stress markers, lipid hydroxide, malondialdehyde and carbonyl in CZM-treated SiHa cells with respect to untreated control sets at two time points of 3 h and 24 h. Data has been presented as mean  $\pm$  SD ( $n=3$ ). \* $P<0.01$ , \*\* $P<0.001$ , \*\*\* $P<0.0001$

### Mitochondrial membrane potential analysis

Mitochondrial membrane potential analysis was done according to Sivandzade et al. 2019.

### Antioxidant assays

#### Non-enzymatic antioxidant content

GSH content was measured as described by Pal et al. 2021.

#### Enzymatic antioxidant activity

Catalase (CAT) and superoxide dismutase (SOD) activities were estimated as described by Pal et al. 2021. Glutathione reductase (GR) (Mannervik 1999), glutathione peroxidase (GPX) (Flohe and Gunzler 1984), glutathione S-transferase (GST) (Pour et al. 2014), thioredoxin reductase (ThR) (Arnér and Holmgren 2000), glutaredoxin (Grx) (Gan and Wells 1986) and peroxiredoxin (Prx) (Veskoukis et al. 2018) activities were estimated according to protocols described in respective references.

### Oxidative marker content estimation

Malondialdehyde (MDA) content was estimated as described by Pal et al. 2021. Lipid hydroperoxide (LOOH) and protein carbonyl content were measured as described by Deiana et al. 1999 and Mesquita et al., 2014, respectively.

### [Ca<sup>2+</sup>] concentration estimation

[Ca<sup>2+</sup>] concentration estimation was done according to Corns and Ludman 1987.

### Estimation of some cellular metabolite contents

Pyruvate (Anthon and Barrett 2003), lactate (Borshchevs-kaya et al. 2016), methylglyoxal (Wild et al. 2012), malate (Hummel 1949) and citrate (Ali et al. 1998) contents were estimated according to protocols mentioned in respective references.

### Estimation of lactate dehydrogenase activity

Estimation of LDH activity was done according to Javed et al. 1997.

### Immunoblotting

Immunoblotting of target proteins was performed following method as described by Majumder et al. 2020. The blots were subjected to NBT/BCIP solution and then visualised in gel documentation unit (Bio-Rad, USA), and polypeptide bands were quantified via Image Lab software (Bio-Rad, v6.0.1).

### Gas chromatography-mass spectroscopic analysis

Gas chromatography-mass spectrometry (GC/MS) analysis was performed as described by Nag et al., 2022.

### High resolution liquid chromatography-mass spectroscopic analysis of plant extract and chromatography fractions

HRLCMS was done according to method described by Pal et al. 2021.

### Silica gel column chromatographic analysis of plant extract

Fractions of CZM were obtained using a silica gel column following the procedure as described by Paul et al., 2019.

### X-Ray diffraction analysis

One crystal each from the two isolated solid fractions obtained from column chromatography of CZM were individually assessed by diffractometer (Bruker SMART APEX II with graphite-monochromated radiation ( $M_{\text{O}}$  K $\alpha$ ),

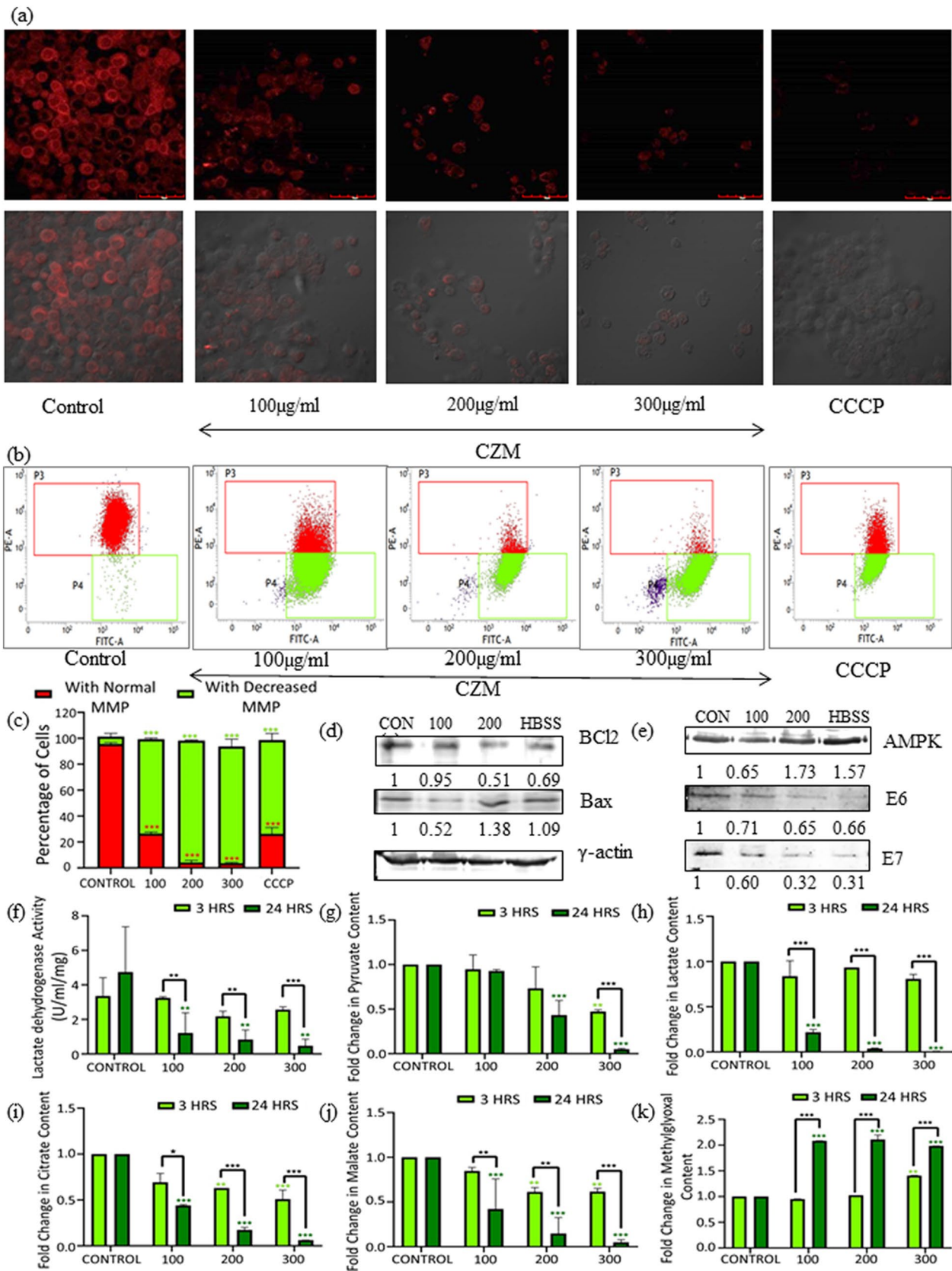




**Fig. 5** CZM affected functional integrity of mitochondria and hampered bioenergetics. **a** Fluorescence microscopy images of Rhodamine 123-stained SiHa cells after treatment of CZM for 3 h showing decrease in mitochondrial membrane potential (MMP) with respect to untreated control set. Scale represents 50  $\mu\text{m}$ . **b** and **c** Histograms and corresponding bar graph, respectively, showing dose-dependent decrease in percentage of red fluorescing population in CZM-treated SiHa cells indicating loss of MMP as detected by flow cytometric analysis. CCCC represents positive control set in both (a) and (b). **d** and **e** Images of immunoblots showing changes in expression of proteins associated with maintaining mitochondrial integrity directly (BC12, Bax) and glycolytic flux indirectly (E6, E7) in CZM-treated SiHa cells.  $\gamma$ -Actin served as loading control. The fold changes in protein expression have been specified below each image of immunoblot. **f** **g** and **h** Estimated lactate dehydrogenase activity, pyruvate and lactate content, respectively, in SiHa cells at 3 h and 24 h application of CZM. **i**, **j** and **k** Estimated citrate, malate and methylglyoxal content in CZM-treated SiHa cells at same time points. Data has been presented as mean  $\pm$  SD ( $n=3$ ). \* $P < 0.01$ , \*\* $P < 0.001$ , \*\*\* $P < 0.0001$

$\lambda = 0.71073 \text{ \AA}$ ). SHELX-97 (Sheldrick-2008) was used to solve the crystal structures to Cambridge Crystallographic Data Centre (CCDC).

## H1 NMR

The  $^1\text{H}$  NMR spectra were recorded in  $\text{CDCl}_3$  solvent at 298 K on a Bruker AM 300L (300 MHz) superconducting FT NMR spectrophotometer.

## Phytochemical content estimation by spectrophotometry

Total phenol, flavonoid, tannin, terpenoid and alkaloid content estimation by spectrophotometry were done according to Singleton and Rossi 1965, Christ and Muller 1960, Broadhurst and Jones, 1978, Ghorai et al. 2012 and Ajanal et al. 2012, respectively.

## Statistical analysis

Experiments have been performed in triplicates. IBM SPSS Statistics Version 21 was used for conducting statistical analyses. Significance of differences was determined using one-way ANOVA and Tukey test in sequence and denoted as \* $P < 0.01$ , \*\* $P < 0.001$  and \*\*\* $P < 0.0001$ .

## Results

### Selective cytotoxicity of CZM in SiHa is dose dependent

Except the CZW, all other extracts of *Curcuma zanthorhiza* were capable of inducing cell death in SiHa though

their cytotoxicity varied. As deduced from MTT reduction assay, CZM was the most potent against SiHa as it showed the lowest  $\text{IC}_{50}$  value of 149.37  $\mu\text{g/ml}$  corresponding to treatment time of 24 h. However, 76.1% HEK293 human embryonic renal cells remained viable when they were treated for 24 h with 150  $\mu\text{g/ml}$  CZM, thus indicating towards the latter's selective cytotoxicity. Depending on the observations made from MTT reduction assay, three doses of CZM (100, 200 and 300  $\mu\text{g/ml}$ ) were chosen for further study.

When CZM-treated SiHa cells were subjected to Trypan blue dye exclusion assay, similar results were observed where around 45% of cells remained non-viable at 100  $\mu\text{g/ml}$  and the non-viability increased with an increase in concentration (Fig. 1).

### CZM attenuates cell proliferation and clonogenicity

Proliferative potential of CZM-treated SiHa cells was also hampered as observed from changes in cell cycle dynamics. There was an increase in sub- $G_0$  cell percentage from  $1.54 \pm 0.46\%$  to  $13.99 \pm 0.31\%$  when subjected to 300  $\mu\text{g/ml}$  CZM for 24 h, while  $G_0$ - $G_1$  decreased from  $73.55 \pm 0.46\%$  to  $47.16 \pm 0.97\%$ , thus indicating anti-proliferative capacity of CZM. Simultaneously, S phase cell percentage increased from  $5.00 \pm 0.94\%$  to  $11.92 \pm 0.7\%$  and  $G_2$ -M phase cells increased from  $17.99 \pm 2.67\%$  to  $23.24 \pm 2.45\%$  pointing towards cell cycle arresting capability of CZM at both S and  $G_2$ -M phases (Fig. 2d, e).

Such disruption of cell cycle was corroborated with nuclear as well as cellular morphological changes as detected by Hoechst 33,258 (Fig. 2a) and Haematoxylin-Eosin staining (Fig. S2), respectively. CZM induced remarkable nuclear condensation as percentage of brightly fluorescing Hoechst-stained nuclei increased from 1.25% in control set to 15.37% in 300  $\mu\text{g/ml}$  CZM-treated set. Similarly, chromosomal erosion became evident with the presence of nuclei with very faint fluorescence. Besides, morphology of SiHa cells altered from spindle-shape to highly condensed and rounded ones.

Halo assay also showed that the halo formed due to nuclear damage, increased in area up to about 73% in 300  $\mu\text{g/ml}$  CZM-treated set compared to the untreated control set after a treatment time of 24 h (Fig. 2b, c).

Exposing SiHa cells to CZM for 24 h hindered their ability to cover wound area markedly in a dose-dependent manner. With respect to control set that filled up 87.06% of the scratch, CZM between 100 to 300  $\mu\text{g/ml}$  covered only 10.69% to 1.97% at the end of 24 h (Fig. 3a, b).

Clonogenicity of SiHa cells also decreased with an increase in dose by 0.47- to 0.09-fold when treated with a tenth of CZM doses for 7 days (Fig. 3c, d).

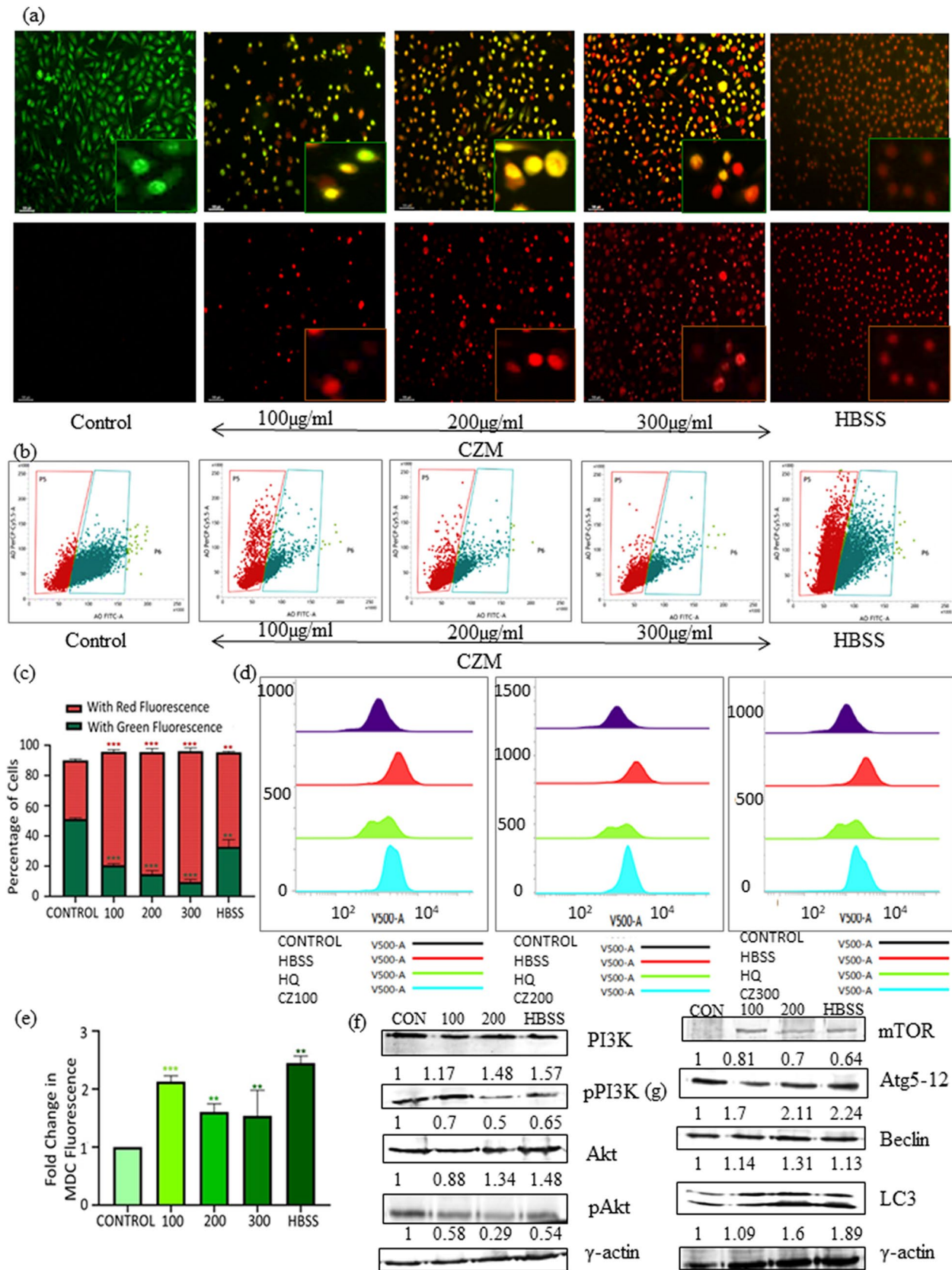


**Fig. 6** CZM induced autophagic cell death in SiHa. **a** Upper panel showing increasing accumulation of acidic compartments (orange-red specks) in acridine orange (AO)-stained SiHa cells treated with CZM for 24 h with respect to untreated control. HBSS represents positive control set. Lower panel showing corresponding fluorescence microscopy images of ethidium bromide (EtBr)-stained cells. Scale represents 100  $\mu$ m. **b** Histograms obtained through flow cytometric analysis showing increase in percentage of red fluorescing AO-stained SiHa cells following treatment with CZM for 24 h, indicating accumulation of acidic vacuoles. **c** Corresponding bar graphs displaying percentage of red and green fluorescing AO-stained CZM-treated SiHa cells as revealed by flow cytometry. **d** Overlay histograms obtained through flow cytometric analysis showing increase in percentage of monodansylcadaverine (MDC)-stained SiHa cells following treatment with CZM for 24 h, indicating autolysosome formation. **e** Corresponding bar graphs displaying percentage of MDC-stained CZM-treated SiHa cells as revealed by flow cytometry. Data has been presented as mean  $\pm$  SD ( $n=3$ ). \* $P<0.01$ , \*\* $P<0.001$ , \*\*\* $P<0.0001$ . **f** Images of immunoblots showing changes in expression of autophagy regulating proteins in CZM-treated SiHa cells **g** Images of immunoblots showing changes in expression of proteins associated with autophagosome formation in CZM-treated SiHa cells.  $\gamma$ -Actin served as loading control. The fold changes in protein expression have been specified below each image of immunoblot. HBSS represents positive control set in all the cases

### CZM destabilised cellular redox homeostasis

CZM-led augmentation of internal ROS level in the targeted sets was clear from microscopic images of DCFDA-stained cells (Fig. 4a). Flow cytometric quantification indicated that at a dose of 300  $\mu$ g/ml the increment was by sevenfold in comparison with control set (Fig. 4b). Pre-incubation with 0.5 mM NAC could decrease accumulation of ROS especially at doses of 100  $\mu$ g/ml and 200  $\mu$ g/ml. RNS level was also found to increase in parallel as NO content got upregulated from 19.5  $\mu$ M at 3 h to about 45.67  $\mu$ M at 24 h (Fig. 4c). Concurrently, the intracellular  $\text{Ca}^{2+}$  concentration also increased from 1.39- to 1.64-fold (Fig. 4d). The antioxidant system got compromised with the assault of the increasing ROS and RNS levels. This was evident as the activity of enzymes like CAT, SOD, GR, GST, GPX, ThR, Grx and Prx diminished in a dose-dependent manner. However, the decrease in activity was more prominent at 24 h. Activities of CAT and SOD were lowered to 2.05 and 0.16 U/ml/mg at 24 h, respectively (Fig. 4e, f), at the highest dose while those of GR, GST and GPX that function in glutathione redox system decreased to 0.37, 0.09 and 0.01 U/ml/mg (Fig. 4g, h, i). The content of non-enzymatic GSH also declined up to 7.32 to 8.21  $\mu$ g/ml (Fig. 4j). Reduction in activities of ThR, Prx and Grx was to 0.03-, 0.54- and 0.09-fold, respectively (Fig. 4k, l, m). The sharp fall in the cellular antioxidant cycle resulted in magnification of levels of oxidative stress markers like LOOH, MDA and carbonyls to 0.18  $\mu$ M/mg, 7.02  $\mu$ M/ml/mg and 0.35 nM/ml/mg, respectively (Fig. 4n, o, p).

### Dysregulated mitochondrial function and imbalance in cellular energy homeostasis

Irregularities in mitochondrial membrane potential of SiHa cells in response to CZM were evident at all the doses. It was visualised through microscopic analysis that the fluorescence of Rhodamine 123-stained cells steadily dropped in a dose-dependent manner with respect to control cells due to the MMP loss (Fig. 5a). Such pronounced impact on MMP was also re-emphasised in flow cytometric analysis that indicated the percentage of cells with red fluorescing JC-1 aggregates depicting the presence of active mitochondria decreased from 95.65% in control set to 3.65% in the highest dose whereas percentage of cells with green fluorescing JC-1 monomers increased from 5.71% to 90.09% showing greater abundance of mitochondria with lowered membrane potential under CZM treatment (Fig. 5b, c). In accordance with this, the expression of Bcl2 and Bax, the two mitochondrial membrane proteins which play pivotal roles in cell survival and death, also changed in comparison with untreated sets as shown in the immunoblots (Fig. 5d). Changes in expression of HPV-associated proteins E6 and E7, which indirectly assist in regulating glycolytic flux, were observed (Fig. 5e). An imbalance in the cellular energy homeostasis was also noticeable in the targeted cells in a time- and dose-dependent decrease in activity of intracellular LDH and lowering of intermediates of aerobic glycolysis like pyruvate and lactate. LDH activity diminished to 3.43 and 16.3 U/ml/mg with respect to control at 3 h and 24 h after CZM application, respectively (Fig. 5f). Pyruvate and lactate concentration lowered to 0.47- and 0.002-fold, respectively (Fig. 5g, h). Concentrations of citrate and malate that are involved in synthesis of important cellular macromolecules also changed. Citrate got reduced to 0.062-fold while malate concentration altered to 0.04-fold (Fig. 5i, j). The upregulated expression of AMPK as observed by immunoblotting also indicated that internal bioenergetics of the CZM-targeted cells got grossly modified (Fig. 5e). Methylglyoxal, a toxic by-product of aerobic glycolysis, increased twice in concentration (Fig. 5k).

### CZM initiated acidic vacuole accumulation and upregulated key autophagic proteins

Fluorescence microscopy as well as flow cytometric analysis revealed greater accumulation of acidic compartments in dose-dependent manner as there was a rise in percentage of red fluorescing cells when stained with AO (Fig. 6a, b). At the highest dosage, percentage of such cells was about 86% which was comparable to 62.85% in HBSS-treated sets (Fig. 6c). MDC staining indicated autophagosome formation in the treated sets got enhanced as the fluorescence increased by 2.12-, 1.6- and 1.53-fold at the three chronological doses (Fig. 6d, e). On co-treatment of 300  $\mu$ g/ml

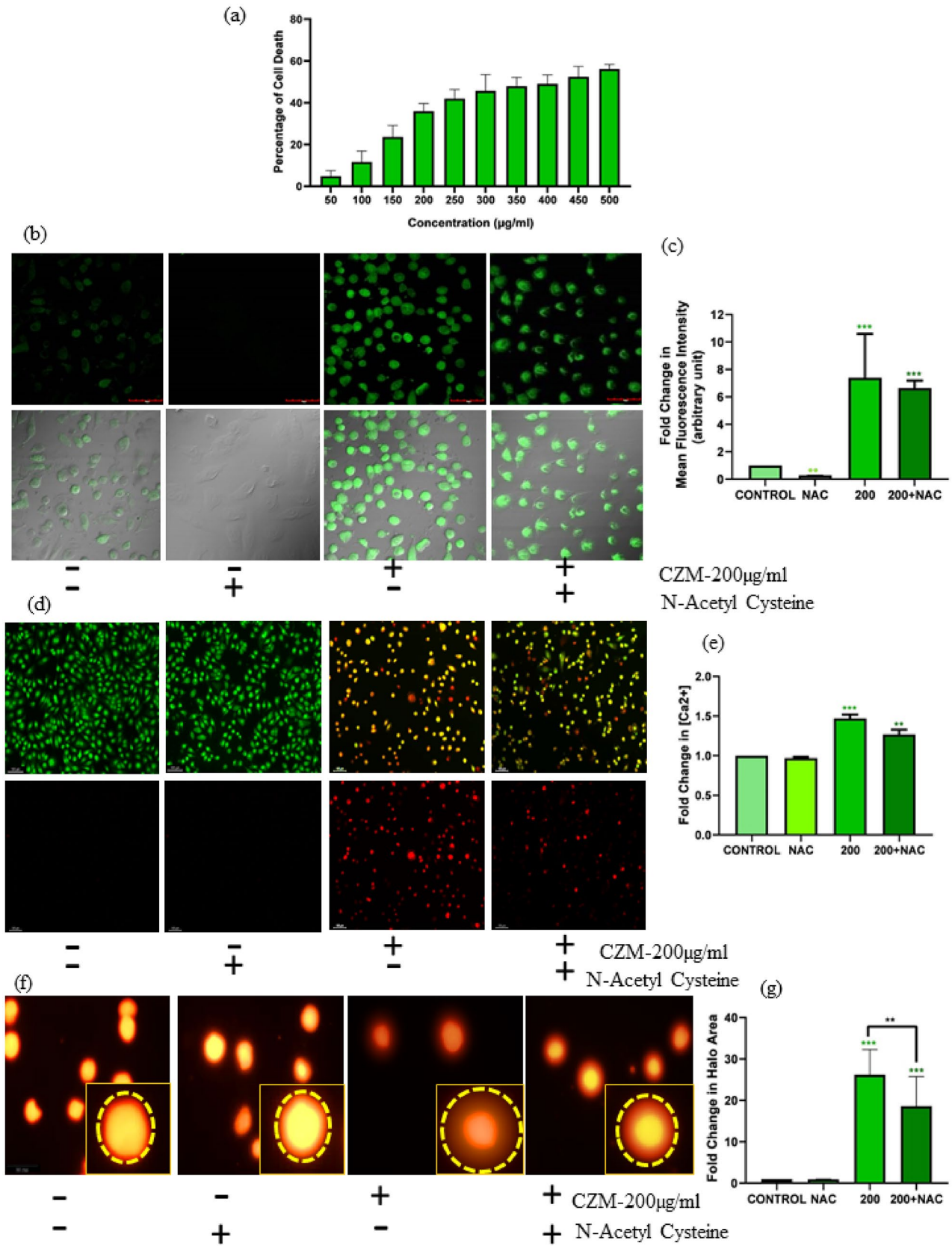


**Fig. 7** NAC exerted partial cytoprotective effect in CZM-treated cells. **a** Bar graph showing changes in cell death percentage in SiHa cells pretreated with NAC (0.5 mM, 30 min) and treated with CZM for 24 h. **b** Confocal microscopy images of DCFDA-stained SiHa cells and **c** corresponding bar graph indicating NAC-mediated lowered CZM-ROS generation induced by CZM. Scale represents 50  $\mu$ m. **d** Fluorescence microscopy images of AO- (upper panel) and EtBr- (lower panel) stained SiHa cells treated with CZM (200  $\mu$ g/ml) and pretreated with NAC. Scale represents 100  $\mu$ m. **e** Bar graph showing changes in intracellular  $[Ca^{2+}]$  content in SiHa cells under same conditions. **f** Fluorescence microscopy images obtained after subjecting NAC-pretreated and CZM-treated SiHa cells to halo assay indicating change in incidence of DNA damage. Representative image for each set has been presented inset. Scale represents 20  $\mu$ m **g** Bar graphs showing percentage changes in area of halo around nuclei with respect to control set. Data has been presented as mean  $\pm$  SD ( $n=3$ ). \* $P < 0.01$ , \*\* $P < 0.001$ , \*\*\* $P < 0.0001$

CZM with hydroxychloroquine (HCQ), it was observed that MDC fluorescence decreased to 1.03-fold, hence confirming that CZM advocated autophagy initiation and promotion in SiHa cells (Fig. S4a). Further immunoblotting showed downregulation in expression of pPI3K and pAKT which function mainly to inhibit onset of autophagy and promote cell survival as well as proliferation (Fig. 6f). Upregulation was also observed in expression of Beclin1, Atg5-12 and LC3II, the key autophagic protein (Fig. 6g).

### NAC can partially rescue the CZM-treated cells

MTT assay indicated that pre-treatment with NAC increased  $IC_{50}$  of CZM by 38% at 24 h (Fig. 7a). Microscopy using DCFDA showed a decrease in ROS level under similar condition (Fig. 7b, c). Microscopy utilising AO/EtBr staining method showed that N-Acetylcysteine (NAC) exercised a partial cytoprotective activity on CZM-treated SiHa cells as percentage of red fluorescing cells decreased to about 25% suggesting lesser accumulation of acidic bodies (Fig. 7d). Simultaneously, EtBr-positive cells were reduced by 15%. Intracellular  $[Ca^{2+}]$  was also reduced to 1.26-fold (Fig. 7e). Halo area around nuclei was observed to be diminished by almost ninefold (Fig. 7f, g). NAC is a synthetic aminothioli precursor of GSH and helps in dissipating excessive ROS and RNS. As NAC was partly successful in averting cell death, it could be stipulated that oxidative stress was largely but not the only responsible factor behind CZM-mediated autophagy in SiHa cells.

### Phytochemical characterisation of CZ extracts

CZ extracted with methanol (CZM), ethyl acetate (CZE), petroleum ether (CZP) and water (CZW) individually were subjected to quantitative spectrophotometric assays, and it was estimated that CZM had the highest total phenol content of about  $157.66 \pm 0.513$  mg GAE/g dry wt. (Fig. 8a) and total flavonoid content was highest in CZE with  $921.29 \pm 0.42$  mg

QE/g dry wt. followed by  $555.81 \pm 0.4$  mg QE/g dry wt. in CZM (Fig. 8b). The greatest total tannin content was found in CZM with  $152.39 \pm 0.494$  mg CE/g dry wt (Fig. 8c). Total terpenoid content was CZM  $7.67 \pm 0.002$  mg LE/g dry wt. (Fig. 8d), and total alkaloid content was about  $5.93 \pm 0.6$  mg SE/g dry wt (Fig. 8e). The petroleum ether and aqueous extracts did not fare well with respect to phytochemical contents. Since CZM was selected for further studies on its cytotoxicity against SiHa, it was put through different mass spectrometric analysis methods. The HRLCMS and GCMS analyses of CZM presented an elaborate picture of its phytochemical profile. Those also confirmed that CZM consists of a range of bioactive phytochemicals (Supplementary Table 1) that belong to diverse phytochemical classes. Chromatograms illustrating their proximation according to the retention times are shown in Fig. 8f, g and h.

### Isolation, identification and characterisation of cytotoxic fractions in CZM against SiHa

The CZM extract yielded several fractions when subjected to silica gel column chromatography. When cytotoxic potential of these fractions was checked through MTT assay, it was found that two fractions (FR-I, FR-II) induced cell death against SiHa with  $IC_{50}$  values of 43.78 and 56.49  $\mu$ l/ml. HRLCMS analysis of FR-I in ESI positive mode showed that it consists majorly of terpenes and terpenoids (41.66%) like cucurbitacin S and isogermafurene and vitamin D3 derivatives (21.49%) while in ESI negative mode indicated the presence of alkaloid (100%) (Fig. 9). GCMS analysis showed that this fraction was made of mainly terpenoids of which the most abundant was xanthorrhizol (44.9%). FR-II was found to be made primarily of esters and fatty acids like ethyl 2E,4Z-hexadecadienoate elaidolinoleic acid and isopalmitic acid amounting to about 81.98% as revealed through HRLCMS done in ESI negative mode (Fig. 9).

Two phytochemicals were also isolated from CZM as pure crystals through column chromatography. One of the crystals has been distinguished as (1E, 6Z)- 1,7-dimethyl-3-oxo-4-(propan-2-ylidene)-2,3,4,5,8,9-hexahydroazeein-1-ium (CCDC Submission ID: 2,082,214), isolated for the first time from *Curcuma zanthorrhiza* Roxb., while the other has been identified as curcumin (CCDC Submission ID: 2,082,213), the marker phytochemical of *Curcuma* species (Fig. 10a, b).  $^1H$  NMR spectra of 2,082,213 (300 MHz,  $CDCl_3$ , 298 K,  $\delta$ /ppm): 7.56–7.62 (d, 1H, H-7,  $J=18$ ), 7.26 (s, 1H, Phenolic -OH), 6.92–7.14 (m, 3H, H-1, H-4, H-5), 6.45–6.50 (d, 1H, H-8,  $J=15$ ), 5.80–5.85 (d, 2H, 2 $\times$ H-10), 3.95 (s, 3H, 3 $\times$ H-11). One singlet peak at 1.55 ppm is due to impurity of  $CH_3Cl$ , came from  $CDCl_3$  solvent used in  $^1H$  NMR (Fig. 10e). Curcumin was found to be most cytotoxic against SiHa with an  $IC_{50}$  value of 25.4  $\mu$ g/ml.

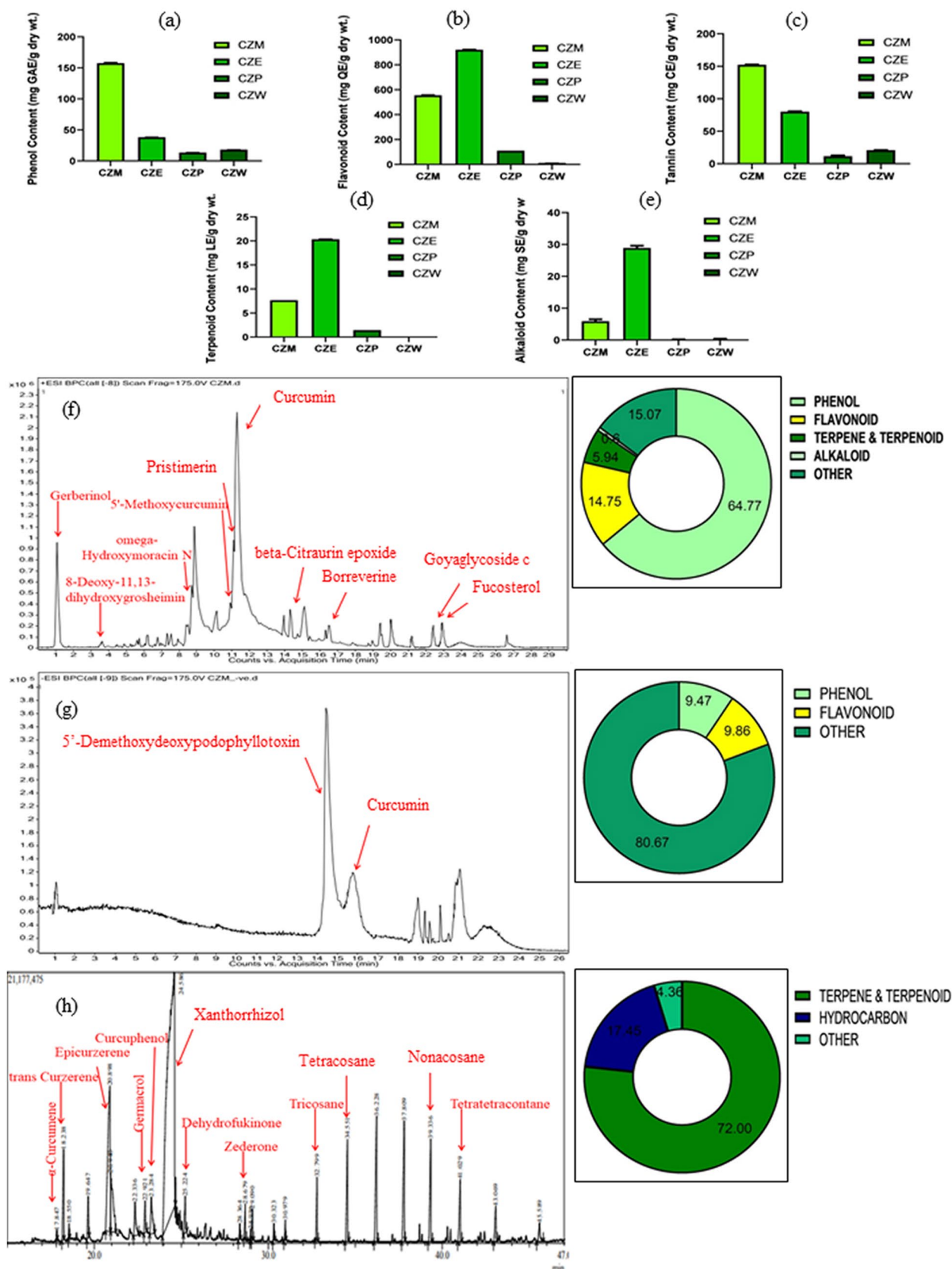


**Fig. 8** Phytochemical composition of CZ extracts. **a** Total phenol content shown as GAE (gallic acid equivalent)/g dry wt. **b** Total flavonoid content shown as QE (quercetin equivalent)/g dry wt. **c** Total tannin content shown as mg CE (catechin equivalent)/g dry wt. **d** Total terpenoid content shown as mg LE (linalool equivalent)/g dry wt. **e** Total alkaloid content shown as mg SE (strychnine equivalent)/g dry wt. **f** and **g** HRLCMS chromatogram (ESI positive and negative modes, respectively) of CZM with corresponding doughnut chart showing contributions of different phytochemical classes in the same. **h** GCMS chromatogram of CZM with corresponding doughnut chart. Phytochemicals of particular interest have been specified in the chromatograms. X-axis denotes the count vs. acquisition time recorded in minutes. Data has been presented as mean  $\pm$  SD ( $n=3$ )

## Discussion

Autophagy has been reported to occur in cancer cells mainly to maintain homeostasis by removing damaged cytosolic organelles and biomolecules. However, under deleterious circumstances such as in the presence of elevated levels of cellular ROS the basal level occurrence of autophagy is found to largely cross over the threshold level, thereby leading to cell death instead of promoting cell survival.

The first distinguished observation upon treatment of SiHa cells with CZM was the increment of both intercellular ROS and RNS levels (Fig. 4). Under normal conditions, these are generally produced via ongoing normal cellular functions. For example, superoxide is formed through actions of cellular enzymes like cytochrome P450 peroxidases, NADPH oxidase and xanthine oxidase (Su et al. 2019). Nitric oxide synthase also acts as a major source of NO.

In order to keep a check on excessive accumulation of these species, the cancer cells possess tightly regulated and largely interconnected redox systems made of enzymatic as well as non-enzymatic antioxidants. The cytosolic zinc and copper-dependent and mitochondrial manganese-dependent superoxide dismutases (SODs) convert superoxide to hydrogen peroxide and oxygen. Catalase of peroxisomes breaks down hydrogen peroxide to form water and molecular oxygen. Among the non-protein thiols in cell, glutathione is more abundant. Reduced glutathione acts as an integral cofactor during the antioxidant reactions requiring exchange of thiol and disulphide groups. The hydroxyl radicals ( $\text{OH}^\cdot$ ) and singlet oxygen get scavenged mainly through these low molecular weight non-enzymatic scavengers. Glutathione reductase (GR) maintains GSSG/GSH concentration ratio in cell as it catalyses NADPH-mediated conversion of oxidised glutathione disulphide (GSSG) to its reduced form. Thioredoxin reductases (TrxRs) are involved mainly in reduction of Thioredoxin (Trx), a redox protein. This occurs in a NADPH-dependent manner (Mustacich and Powis 2000). The TrxR/Trx system also sustains the GSH pools besides the GR. Glutathione peroxidase, a selenoenzyme present

in mitochondria and cytosol, detoxifies lipid peroxides and  $\text{H}_2\text{O}_2$  through electron-donating activity of GSH (Jiao et al. 2017). Glutathione S-transferases (GSTs) play role in conjugating the GSH to different exogenous as well as endogenous reactive electrophile components and thus protect the macromolecules in cell (Townsend et al. 2003). Peroxiredoxins participate in reducing lipid hydroperoxides (LOOH) and scavenging hydrogen peroxides present in free state while electrons get withdrawn from thioredoxin. Glutaredoxins are also proteins with sulfhydryl groups and cooperate with the Trx system via hydrogen donation (Vernis et al. 2017). However, the redox system of SiHa cells when treated with CZM has been found to be dysregulated as activities of the different antioxidant enzymes diminished while concentration of non-enzymatic antioxidant GSH also got lowered (Fig. 4).

The resultant imbalance got exacerbated in a time-dependent manner and ultimately led to a total collapse of the redox homeostasis. It is known that the reactive oxygen and nitrogen species associate among themselves to form more such components as themselves. On the other hand, they interact with the macromolecules and affect the latter.  $\text{H}_2\text{O}_2$  reacts with nitrite to form free radical of nitrogen dioxide.  $\text{OH}^\cdot$  aggressively and unselectively oxidises DNA bases and disturbs the double helix. Singlet oxygen engages with proteins by oxidising their side chains and causes their conformational changes. NO in the presence of  $\text{O}^\ominus$  converts to peroxynitrite that creates the unstable lipid nitrate intermediates. Thus, adverse rise in ROS levels leads to formation of noxious adducts of different cellular biomolecules. The free radicals extricate electrons from lipids to form further reactive intermediates like lipid hydroperoxides and malondialdehyde. The cellular and organellar membranes with more polyunsaturated fatty acids are more sensitive to such lipid peroxidation (Su et al. 2019). Similarly, proteins get oxidised to form harmful carbonyls. The build-up of ROS and RNS in the CZM-treated SiHa cells due to the progressive inactivation of cellular redox system also led to increased concentration of different oxidative stress markers such as lipid hydroperoxides, malondialdehyde and protein carbonyls (Fig. 4). These in turn inflict further damage to the cell.

Of these, the lipid hydroperoxides (LOOH) affect more seriously, since, when decomposed through reduction via one-electron system they lead to further propagation of chain reactions that again continue peroxidation of other lipids. The LOOHs react with oxygen radicals to form peroxy ( $\text{LOO}^\cdot$ ) and alkoxy ( $\text{LO}^\cdot$ ) radicals. Lipids constitute about 50% of the cell membrane. The accumulation of deleterious lipid adducts alters fluidity of biomembranes resulting in a harsh drop in membrane integrity and eventual malfunctioning of membrane proteins. Such loss of membrane integrity in the treated sets was evident from the dose-dependent increase in percentage of the Trypan blue-positive cells (Fig. 1).

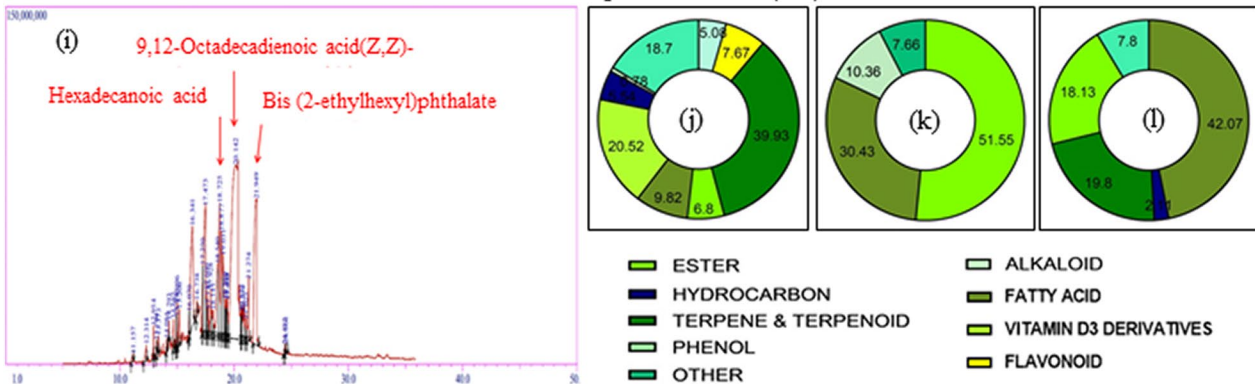
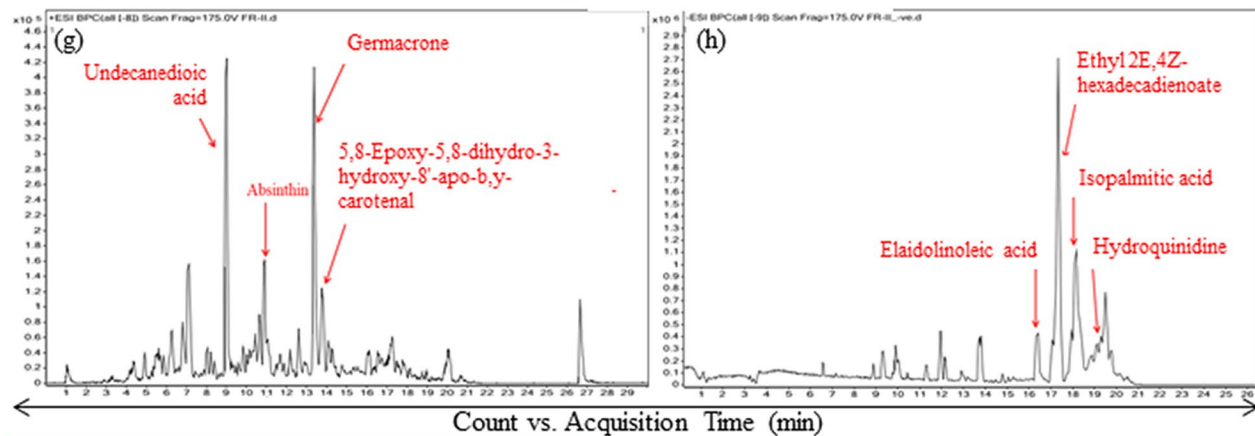
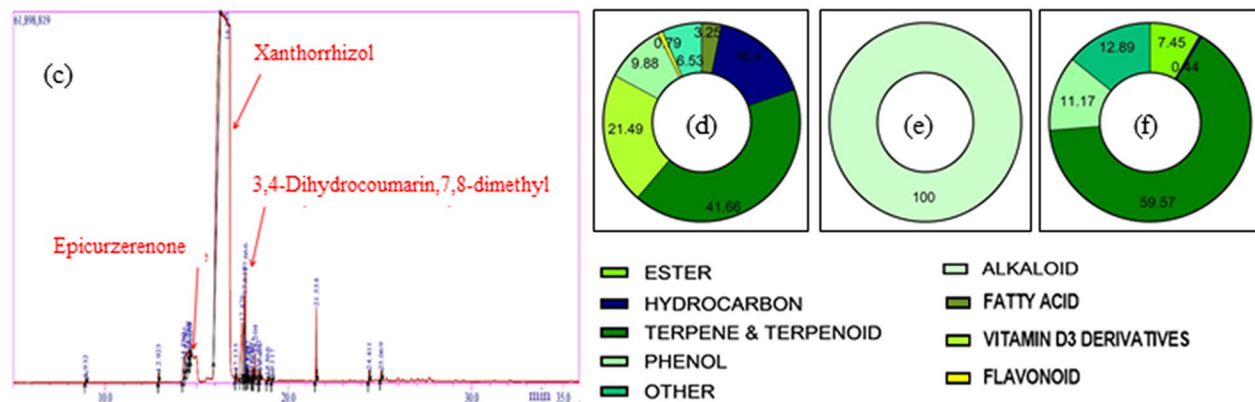
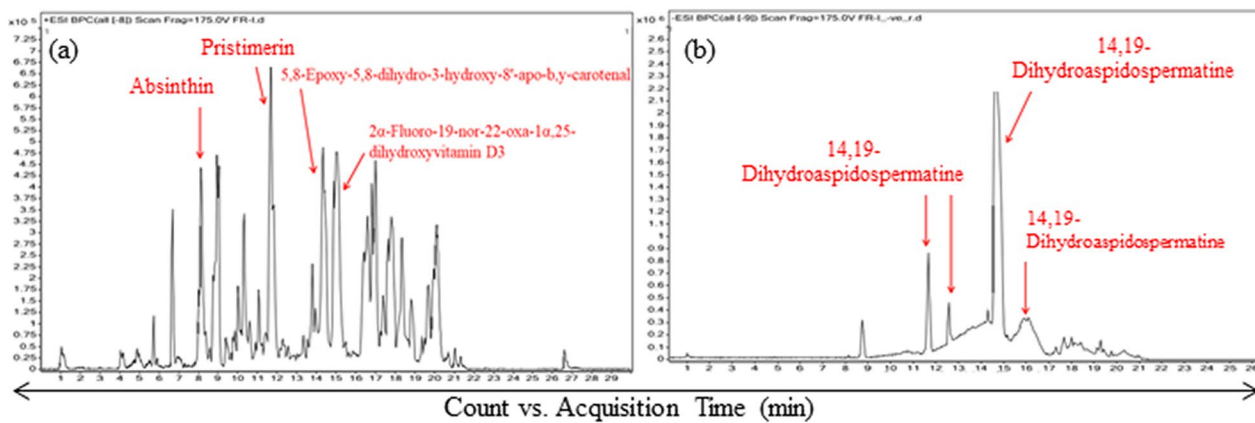




**Fig. 9** Biomolecular characterisation of the two cytotoxic fractions obtained from CZM through silica gel column chromatography. **a** and **b** Chromatograms showing peaks of various phytochemicals present in FR-I obtained via HRLCMS analysis done in ESI positive and negative modes, respectively. X-axis denotes the count vs. acquisition time recorded in minutes. **c** Chromatogram obtained after GCMS analysis of FR-I. **e**, **f** and **g** Doughnut charts showing contributions of different classes of phytochemicals in the FR-I as detected through HRLCMS (ESI positive, ESI negative) and CMS analyses. Phytochemicals of particular interest have been specified in the chromatograms. **h** and **i** Chromatograms showing peaks of various phytochemicals present in FR-II obtained via HRLCMS analysis done in ESI positive and negative modes, respectively. **j** Chromatogram obtained after GCMS analysis of FR-II. **k**, **l** and **m** Doughnut charts showing contributions of different classes of phytochemicals in the FR-II

Oxidation of nucleic acids also impacts the cells negatively as oxidised nuclear material (like 8-oxo-G) can directly indulge in chromosomal erosion as it hinders telomeric protein from binding to DNA, interferes with telomerase action and thus inhibits end-capping of chromosomes (Perillo et al. 2020). Occurrence of such oxidised bases poses more problems to mitochondrial DNA since the latter lacks protection rendered by histones as well as the enzymatic nucleotide excision repair system. Incidence of chromosomal erosion was noticeable as the number of faintly fluorescing Hoechst-stained nuclei of treated sets got raised with the doses and the diameter of the nuclear halos as visualised via halo assay also increased (Fig. 3). Apart from maintaining the redox balance, the redox systems of the cell coordinate and contribute together either directly or indirectly to preserve numerous critical cell survival functions. For instance, Trx helps in activating ribonucleotide reductase that aids in DNA replication as well as DNA repair mechanisms through formation of deoxyribonucleotides. Glutaredoxins are known to participate during biosynthesis of DNA. They also perform during biogenesis of Fe-S clusters which are involved in continuing functions of DNA polymerases, DNA primase and glycosylases (Vernis et al. 2017). Thus, functional dysregulation of the redox system is capable of negatively affecting cell cycle dynamics and proliferative potential of cell. This is supported by disruption of cell cycle progression and proliferation in SiHa cells in response to CZM (Fig. 3).

Besides nucleus, mitochondria were also imposed with the injurious influences of the unabated piling of cellular ROS, as was implied by a lowering of mitochondrial membrane potential in the cells treated with CZM (Fig. 5). Furthermore, the disturbed status of Bax and Bcl2 proteins' equilibrium as observed from the immunoblots also pointed towards the mitochondrial damage. Mitochondrial membrane phospholipids when affected by the ROS often lead to disaggregation of Complex I and III, increase leakage of electrons within the intermembrane space and decrease membrane potential (Perillo et al. 2020).

With a hike in mitochondrial depolarization, a derailment in bioenergetics becomes inevitable as observed in this study. Cancer cells exhibit high rate of fatty acid synthesis with an equally high rate of mitochondrial  $\beta$ -oxidation for fatty acid catabolism. The catabolic products are necessary for protecting unattached cancer cells from death by anoikis and aiding a better cell migration process (Li et al. 2021). In all probability, with the absence of soundly functioning mitochondria in bulk within the affected SiHa cells, the  $\beta$ -oxidation process got hindered. This can be a cause for the stalled migratory potential of the targeted cells, besides the fact that curcumin, the major flavonoid present in CZM in an appreciable quantity, is known to inhibit functions as well as expressions of different matrix metalloproteinase proteins (Bachmeier et al. 2018).

HPV infection induces several alterations in the metabolic profile of the cell, of which the most prominent is the change in glycolytic flux. In the highly proliferative cancer cells, Warburg effect is chiefly observed wherein they generate ATP through aerobic glycolysis bypassing the mitochondrial oxidative phosphorylation and produce lactic acid. E6, an important 'oncoplayer' in SiHa cells, secures c-Myc from disintegration through o-linked-N-acetylglucosaminylation and helps in upregulation of hexokinase-2 (HK2) transcription. It also renders p53 inactive which in turn leads to downregulation of miR-34a that inhibits activity of LDHA whose primary function is to convert pyruvate to lactate. Thus, E6 promotes aerobic glycolysis in infected cervical cancer cells as HK2 acts as a key enzyme of glycolysis. E6/E7 also downregulate expression of miR-143-3p that normally keeps glycolytic flux under check by opposing HK2 expression. In the CZM-treated SiHa cells, it was detected that intracellular LDH activity decreased with time while the concentrations of both pyruvate and lactate dropped (Fig. 5). One of the underlying reasons for this might be the downregulation of E6 and E7 expressions in the targeted cells as observed from immunoblot analysis. The lowering of phosphorylated AKT also supports considerable obstruction to the occurrence of glycolysis since AKT hyperactivation as is seen in HPV-positive cells is the major contributor in activating the leading glycolytic enzymes like phosphofructokinase and overexpression of membrane glucose transporters like GLUT1 (Li and Sui 2021). The resultant loss of energy homeostasis in the cells was also apparent from the reduction of intermediates like citrate which is required for cholesterol and fatty acid synthesis in cytoplasm (Koundouros and Poulgiannis 2020) and malate which is essential for amino acid biosynthesis.

The unavoidable bane of aerobic glycolysis is formation of methylglyoxal which is an unstable, electrophilic dicarbonyl compound. It associates chiefly with the basic amino acids of protein molecules to produce hazardous advanced glycation end products (AGEs). Under normal conditions,

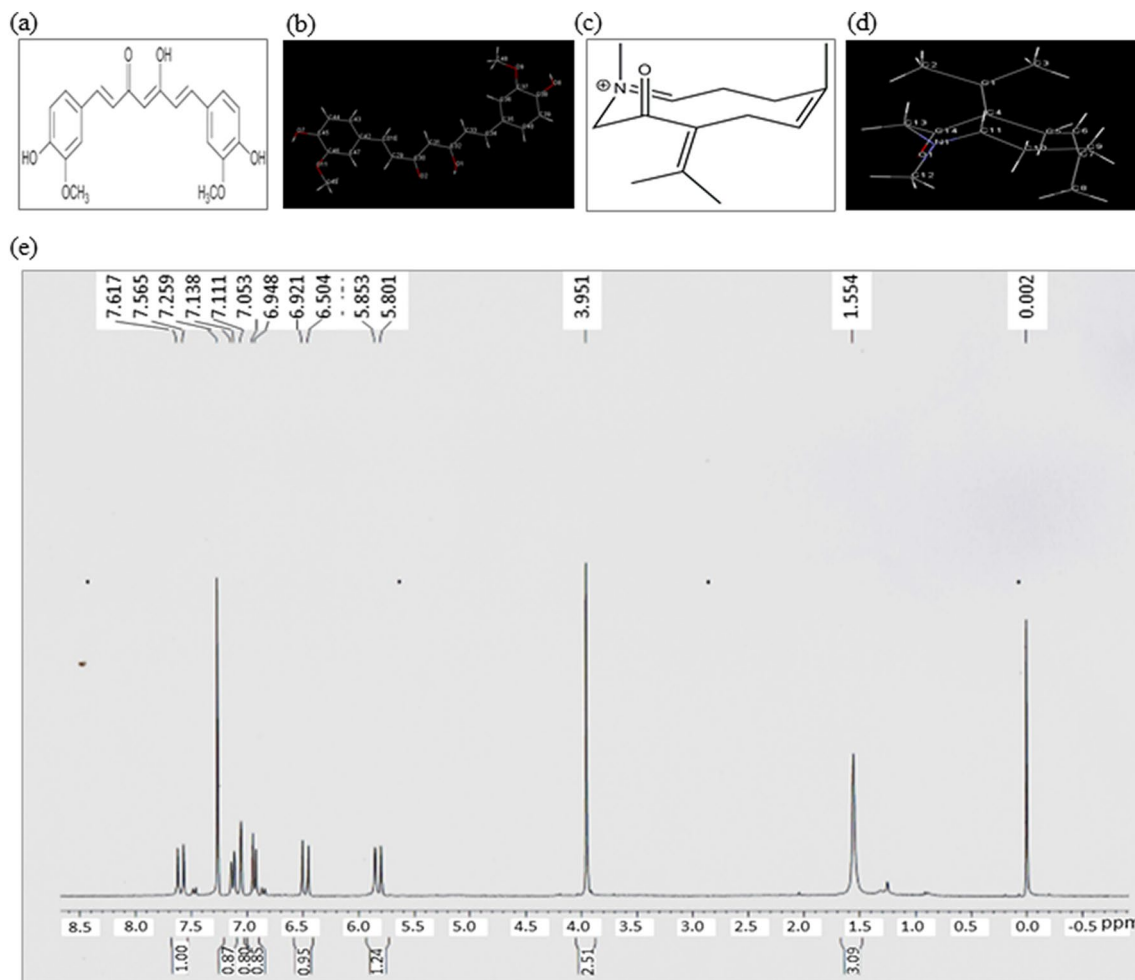


**Fig. 10** Characterisation of crystals isolated from CZM through silica gel column chromatography. **a** 2-dimensional structure of (1E, 6Z)-1,7-dimethyl-3-oxo-4-(propan-2-ylidene)-2,3,4,5,8,9-hexahydroazeein-1-ium (CCDC Submission ID: 2,082,214). **b** Corresponding 3-dimensional crystallographic structure analysed by XRD method.

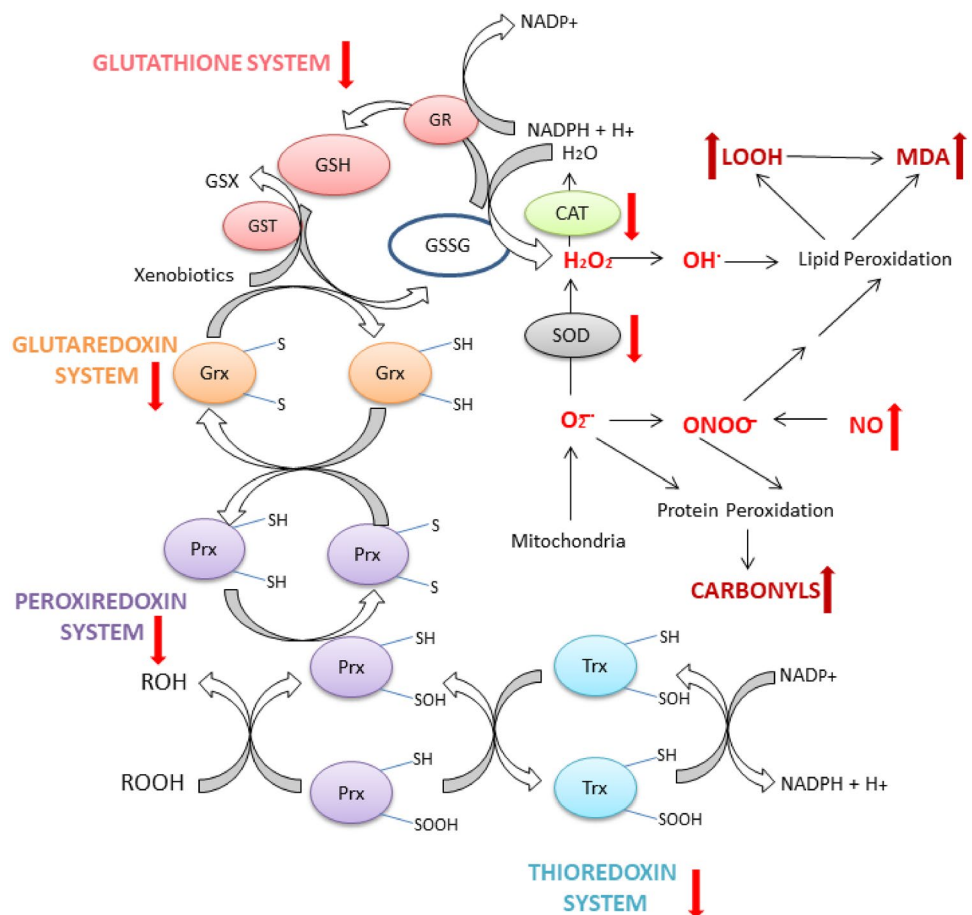
**c** 2-dimensional structure of curcumin (CCDC Submission ID: 2,082,213). **d** Corresponding 3-dimensional crystallographic structure analysed by XRD method. **e** 1H NMR spectrum of curcumin isolated from CZM

methylglyoxal gets detoxified by glyoxalases (GLO) in the presence of GSH and GSH-linked enzymes like GR and GPx. In the absence of properly operational GLO/GSH axis, methylglyoxal accumulates in the cell and initiates cytotoxicity. In HT22 nerve cells, methylglyoxal treatment for 18 h resulted in an increase in Trx1 loss, the activation of AMPK, a decrease in phosphorylation of mTOR and an increase in active LC3, all indicating towards onset of autophagy (Dafre et al. 2017). In retinal ARPE-19 cells, methylglyoxal leads to an increment in autophagy flux and inhibits cell proliferation (Chang et al. 2015). In this study, the concentration of methylglyoxal has been found to increase in time-dependent manner and it might be one of the factors responsible for inducing autophagy in the CZM-treated cells.

The process of autophagy starts with the formation of autophagosome, a double membrane-bound vesicle to

internalise targeted cellular components, followed by fusion with lysosome, and culminates with degradation through the hydrolytic enzymes. Microscopic and flow cytometric analyses indicated towards dose-dependent escalation of autophagic attack on SiHa cells by CZM since the proportion of cells stained with AO and MDC increased. Beclin1, a crucial member that when active, participates in autophagosome initiation and maturation, remains bound through its BH3 domain to inhibitory BCL2. Expression of Beclin1 also increased with a concomitant decrease of BCL2. Bax which has been reported to enhance autophagy through lysosomal membrane permeabilization also got upregulated. LC3II, the biomarker of autophagy, and Atg5-12 which is required for LC3II maturation showed an amplified expression in both treated and positive control sets. It is the phosphatidylethanolamine conjugate of cytosolic LC3 that is induced

**Fig. 11** CZM destabilised redox homeostasis of SiHa cells by adversely affecting the intercellular antioxidant defence system comprising interconnected cycles of glutathione, glutaredoxin, peroxiredoxin and thioredoxin. This resulted in an increase in levels of ROS and different oxidative stress markers in the target cells



to nascent phagophore membrane and gets degraded by lysosomal enzymes when autophagosome merges with lysosome to form autolysosome. Thus, this turnover of LC3II indicates a properly functioning autophagic activity. Hydroxychloroquine inhibits autophagic flux by disorganizing Golgi-endolysosome system and preventing fusion between autophagosome and lysosome, without affecting acidity of the latter (Mauthe et al. 2018). Application of HCQ and resultant rise in both LC3II expression and percentage of MDC-positive cells also pointed towards induction of autophagy by CZM. Oxidative stress and subsequent injury seem to be the major underlying causes for this initiation of autophagy since with application of antioxidant NAC the cytotoxicity of CZM to SiHa diminished to some extent. Enhanced internal ROS level is capable of activating AMPK which in turn inhibits anti-autophagic mTOR via monitoring the TSC1/TSC2/Rheb axis and simultaneously phosphorylates ULK1 so that the latter can properly function as the key scaffold protein to trigger autophagosome maturation. pPI3K phosphorylates the downstream protein AKT which then activates mTOR to inhibit autophagy. It was observed that in the CZM-treated as well as nutrient-starved cells expression of pPI3K and pAKT decreased while those of AMPK and mTOR increased. Elevated ROS

also oxidises the cysteine protease Atg4 which initiates and promotes formation of LC3II (Zhang et al. 2016). Further, the magnified ROS and ensuing membrane depolarisation activate lysosomal TRPML1 channels which trigger Ca<sup>2+</sup> release from lysosomes. The rise in Ca<sup>2+</sup> concentration prompts transcription of genes involved in calcineurin-activated and TFEB-mediated induction of autophagy and co-ordinated biogenesis of lysosomes. Primarily, the high [Ca<sup>2+</sup>] amplifies autophagic rate in a two-pronged manner. On one hand, it signals activation of AMPK via CaMMKβ while on the other it prompts DAPK to phosphorylate BCL2, thereby rendering Beclin1 free to participate in autophagosome formation. Thus, it is likely that the leap in [Ca<sup>2+</sup>] in CZM-treated cells in response to enhanced ROS also contributed to orchestrating autophagic cell death.

The potential of CZM regarding onset of autophagy in SiHa due to loss of redox homeostasis, sequential upswing in oxidative stress (Fig. 11) and eventual inactivation of PI3K/AKT/mTOR (Fig. 12) signalling cascade can be justified by the presence of an array of phytochemicals that can function in a similar manner. Quantitative phytochemical characterisation revealed the presence of phenols, flavonoids, terpenoids, alkaloids, tannins, etc., in CZM, and this was validated by HRLCMS and GCMS analyses also. The

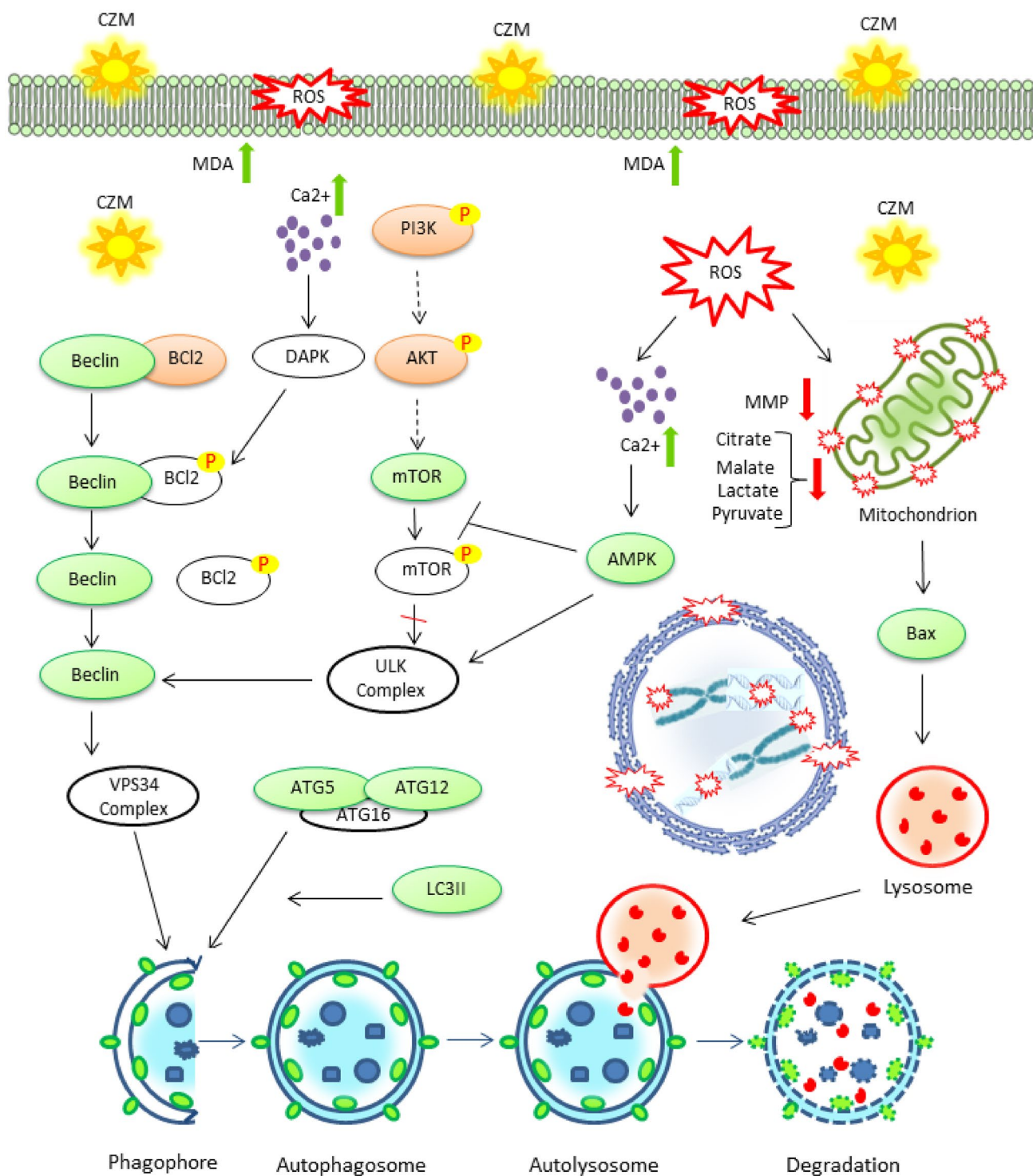


**Fig. 12** Probable mode of action of CZM on SiHa cells represented schematically. CZM increased the intercellular ROS that in turn affected the lipid bilayer, mitochondria and nucleus leading to increase in lipid peroxidation product, i.e. MDA, decrease in mitochondrial membrane potential and condensation and erosion of nuclear material. CZM also decreased concentration of cellular metabolites like citrate, malate, lactate and pyruvate and increased concentration of calcium. The high calcium level phosphorylated BCL2 probably via DAPK, and thus, Beclin was set free to initiate autophagosome formation probably through VPS34 complex. CZM

also increased expression of Atg5-12 and LC3II that also helped in autophagosome formation. AMPK contributed by inhibiting mTOR phosphorylation and activating Beclin through ULK complex. Further mTOR was inactivated through inhibition of PI3K/AKT. Lysosome fused with autophagosome to form autolysosome while activated Bax from damaged mitochondria aided in proper functioning of lysosome. Proteins marked in green were upregulated, those in red were downregulated, and colourless ones were not experimentally studied here

notable phytochemicals that probably helped in cytotoxicity of CZM and their bioactivities have been discussed in Supplementary Table 5. Silica gel column chromatography of CZM led to separation of two crystal compounds and five fractions. Of these, curcumin was observed to have lowest  $IC_{50}$  value against SiHa as deduced from MTT assay (Fig. S3) and can be concluded as the major bioactive phytochemical present in CZM.

It will be important for future research to clarify the relevance of the aryl hydrocarbon receptor (AhR) in the beneficial effects of Java Ginger, given the importance of the AhR in the pathophysiology of most cancers, including cervical cancers (Wang et al. 2021), as well as the role of the AhR driving the 'exhaustion' in natural killer cells and CD8 + T cells, and therefore altering the interaction of the cancer cells with immune cells in the tumour microenvironment (Anderson 2020). The AhR has recently been proposed as a marker of poor prognosis in cervical cancers (Wang et al. 2021). This may link to the data above given the role of the PI3K/Akt pathway in the inhibition of glycogen synthase kinase (GSK3 $\beta$ ), with active GSK3 $\beta$  involved in the degradation of the AhR, as shown in cervical cancer cell lines and other cancers (Yang and Chan 2021). On the other hand, AhR, via the induction of cytochrome P4501B1 (CYP1B1), also 'backward' converts melatonin to N-acetylserotonin (NAS). This NAS in turn activates the Tropomyosin receptor kinase B (TrkB), thereby increasing the proliferation and survival of cancer cells and cancer stem cells (Anderson 2019). It was earlier reported that curcumin can act as a potential target of AhR in anti-inflammatory signalling pathway, as LPS-induced IL6 and TNF  $\alpha$  were attenuated in curcumin-treated rat astrocytes (Lin et al. 2022). It will be interesting to determine as to how the Java Ginger extract and especially the curcumin in it is interacting with these proliferation and inflammatory processes via AhR activity alteration.

## Conclusion

Thus, in conclusion, this study demonstrates that sesquiterpenoid-rich rhizome extract of the nutritious *Curcuma zanthorrhiza* Roxb. possesses merit as a natural agent having selective cytotoxicity against SiHa cervical cancer cells. The observations also pointed towards the dose-dependent anti-migratory and anti-clonogenic activities of the same which further accentuate its anti-proliferative property. The alteration in the PI3K/AKT/mTOR pathway and destabilisation of intracellular redox defence mechanism, as depicted through lowered activity of different enzymatic antioxidant systems and decreased level of non-enzymatic thiols, acted in a feedback loop to trigger cell membrane damage, nuclear material degradation and mitochondrial function impairment. Besides,

downregulation of the HPV-marker proteins E6 and E7 also aided in the process and bruised the bioenergetic homeostasis of the cells. The cumulative outcome of such injuries mediated by the extract ultimately expedited autophagic cell death in the SiHa cells. Thus, this report provides preliminary evidence supporting the traditional use of the plant by the indigenous Java tribes against gynaecological tumours associated with cervical cancer. Further, the phytochemical repertoire of *Curcuma zanthorrhiza* as detected through mass spectroscopic and column chromatographic analyses validated the versatility of this salient Zingiberaceous plant of immense ethnomedicinal importance. Although its ability to bring about death in other cancer cell types has not been highlighted here, yet the circuit of its mode of action as presented may help in future research to establish the plant as an effective and safe anti-cancer arsenal and enhance its position as a functional food.

**Supplementary Information** The online version contains supplementary material available at <https://doi.org/10.1007/s13205-022-03415-9>.

**Acknowledgements** SN would like to acknowledge Prof. Mamiyil Sabu, University of Calicut for kindly providing the rhizome of *Curcuma zanthorrhiza* Roxb. SAIF-IIT Bombay is acknowledged for HRLCMS analyses, University of Calcutta's CRNN for allowing use of flow cytometer, DBT-IPLS facility for confocal microscope, UGC-UPE facility for gel-documentation unit. SN would like to thank all the former and present research scholars from Advanced Cell Biology Laboratory, Department of Botany, University of Calcutta, for their help. This work was supported by University Grants Commission-Universities with Potential for Excellence (UGC-UPE)-II, Grant number: UGC/144/UPE/ST1 (20.03.17). SN thanks the University Grants Commission, Government of India for her fellowship.

**Author contribution** SN and RK conceived the work. SN carried out the experiments and curated data. DP conducted NMR and helped with NMR and XRD analyses. AN conducted GCMS procedure and SN analysed the data. SN wrote the manuscript. RK assessed and confirmed the manuscript.

**Data availability** Data will be available on reasonable request to corresponding author.

## Declarations

**Conflict of interest** The authors declare that they have no known competing interests.

## References

- Ajanal M, Gundkalle MB, Nayak SU (2012) Estimation of total alkaloid in Chitrakadivati by UV-Spectrophotometer. *Ancient Sci. Life* 31:198–201. <https://doi.org/10.4103/0257-7941.107361>
- Anderson G (2019) Breast cancer: occluded role of mitochondria N-acetylserotonin/melatonin ratio in co-ordinating pathophysiology. *Biochem Pharmacol* 168:259–268. <https://doi.org/10.1016/j.bcp.2019.07.014>
- Anderson G (2020) Tumour microenvironment: roles of the aryl hydrocarbon receptor, O-GlcNAcylation, acetyl-CoA and melatonergic pathway in regulating dynamic metabolic interactions

- across cell types-tumour microenvironment and metabolism. *Int J Mol Sci* 22(1):141. <https://doi.org/10.3390/ijms22010141>
- Anthony GE, Barrett DM (2003) Modified method for the determination of pyruvic acid with dinitrophenylhydrazine in the assessment of onion pungency. *J Sci Food Agric* 83(12):1210–1213. <https://doi.org/10.1002/jsfa.1525>
- Arner ES, Holmgren A (2000) Physiological functions of thioredoxin and thioredoxin reductase. *Eur J Biochem* 267(20):6102–6109. <https://doi.org/10.1046/j.1432-1327.2000.01701.x>
- Bachmeier BE, Killian PH, Melchart D (2018) The role of curcumin in prevention and management of metastatic disease. *Int J Mol Sci* 19(6):1716. <https://doi.org/10.3390/ijms19061716>
- Borshchevskaya LN, Gordeeva TL, Kalinina AN, Sineokii SP (2016) Spectrophotometric determination of lactic acid. *J Anal Chem* 71(8):755–758. <https://doi.org/10.1134/S1061934816080037>
- Broadhurst RB, Jones WT (1978) Analysis of condensed tannins using acidified vanillin. *J Sci Food Agric* 29:788–794. <https://doi.org/10.1002/jsfa.2740290908>
- Chang YC, Hsieh MC, Wu HJ, Wu WC, Kao YH (2015) Methylglyoxal, a reactive glucose metabolite, enhances autophagy flux and suppresses proliferation of human retinal pigment epithelial ARPE-19 cells. *Toxicol in Vitro* 29(7):1358–1368. <https://doi.org/10.1016/j.tiv.2015.05.014>
- Chiruvella KK, Panjamurthy K, Choudhary B, Joy O, Raghavan SC (2010) Methyl angolensate from callus of Indian redwood induces cytotoxicity in human breast cancer cells. *Int J Biomed Sci* 6(3):182. <https://doi.org/10.1016/j.febslet.2008.11.001>
- Christ B, Müller KH (1960) Zur serienmäßigen Bestimmung des gehaltes an flavonol-derivaten in drogen. *Arch Pharm* 293(12):1033–1042
- Corns CM, Ludman CJ (1987) Some observations on the nature of the calcium-cresolphthalein complexone reaction and its relevance to the clinical laboratory. *Ann Clin Biochem* 24(4):345–351. <https://doi.org/10.1177/000456328702400403>
- Dafre AL, Schmitz AE, Maher P (2017) Methylglyoxal-induced AMPK activation leads to autophagic degradation of thioredoxin 1 and glyoxalase 2 in HT22 nerve cells. *Free Radic Biol Med* 108:270–279. <https://doi.org/10.1016/j.freeradbiomed.2017.03.028>
- Deiana M, Aruoma OI, Maria de Lourdes PB, Spencer JP, Kaur H, Halliwell B, Aeschbach R, Banni S, Dessi MA, Corongiu FP (1999) Inhibition of peroxynitrite dependent DNA base modification and tyrosine nitration by the extra virgin olive oil-derived antioxidant hydroxytyrosol. *Free Radic Biol Med* 26(5–6):762–769. [https://doi.org/10.1016/s0891-5849\(98\)00231-7](https://doi.org/10.1016/s0891-5849(98)00231-7)
- Franken NA, Rodermond HM, Stap J, Haveman J, Van Bree C (2006) Clonogenic assay of cells in vitro. *Nat Protoc* 1(5):2315–2319. <https://doi.org/10.1038/nprot.2006.339>
- Gan ZR, Wells WW (1986) Purification and properties of thioltransferase. *J Biol Chem* 261(3):996–1001. [https://doi.org/10.1016/S0021-9258\(17\)36043-X](https://doi.org/10.1016/S0021-9258(17)36043-X)
- Ghorai N, Chakraborty S, Guichait S, Saha SK, Biswas S (2012) Estimation of total terpenoids concentration in plant tissues using a monoterpene, linalool as standard reagent. *Protoc Exch*. <https://doi.org/10.1038/protex.2012.055>
- Hummel JP (1949) The fluorometric determination of malic acid. *J Biol Chem* 180(3):1225–1228. [https://doi.org/10.1016/S0021-9258\(19\)51235-2](https://doi.org/10.1016/S0021-9258(19)51235-2)
- Ismail N, Pihie AHL, Nallapan M (2005) Xanthorrhizol induces apoptosis via the up-regulation of bax and p53 in HeLa cells. *Anticancer Res* 25(3B):2221–2227
- Jantan I, Rohani AS, Sumantri IB (2021) Immunomodulatory effects and mechanisms of curcuma species and their bioactive compounds: A review. *Front Pharmacol* 12:643119. <https://doi.org/10.3389/fphar.2021.643119>
- Javed MH, Azimuddin SM, Hussain AN, Ahmed A, Ishaq M (1997) Purification and characterization of lactate dehydrogenase from Varanus liver. *Exp Mol Med* 29(1):25–30. [https://doi.org/10.1016/0305-0491\(94\)00230-r](https://doi.org/10.1016/0305-0491(94)00230-r)
- Kim AJ, Kim YO, Shim JS, Hwang JK (2007) Immunostimulating activity of crude polysaccharide extract isolated from *Curcuma xanthorrhiza* Roxb. *Biosci Biotechnol Biochem* 71(6):1428–1438. <https://doi.org/10.1271/bbb.60241>
- Koundouros N, Pouligiannis G (2020) Reprogramming of fatty acid metabolism in cancer. *Br J Cancer* 122(1):4–22. <https://doi.org/10.1038/s41416-019-0650-z>
- Li B, Sui L (2021) Metabolic reprogramming in cervical cancer and metabolomics perspectives. *Nutr Metab* 18(1):1–14. <https://doi.org/10.1186/s12986-021-00615-7>
- Liang CC, Park AY, Guan JL (2007) In vitro scratch assay: a convenient and inexpensive method for analysis of cell migration in vitro. *Nat Protoc* 2(2):329–333. <https://doi.org/10.1038/nprot.2007.30>
- Lin CH, Chou CC, Lee YH, Hung CC (2022) Curcumin facilitates aryl hydrocarbon receptor activation to ameliorate inflammatory astrogliosis. *Molecules* 27(8):2507. <https://doi.org/10.3390/molecules27082507>
- Majumder I, Paul S, Nag A, Kundu R (2020) Chloroform fraction of *Chaetomorpha brachygonia*, a marine green alga from Indian Sundarbans inducing autophagy in cervical cancer cells in vitro. *Sci Rep* 10(1):1–12. <https://doi.org/10.1038/s41598-020-78592-9>
- Mannervik B (1999) Measurement of glutathione reductase activity. *Curr Protoc Toxicol* 1:7–2. <https://doi.org/10.1002/0471140856.tx0702s00>
- Mauthe M, Orhon I, Rocchi C, Zhou X, Luhr M, Hijlkema KJ, Coppes RP, Engedal N, Mari M, Reggiori F (2018) Chloroquine inhibits autophagic flux by decreasing autophagosome-lysosome fusion. *Autophagy* 14(8):1435–1455. <https://doi.org/10.1080/15548627.2018.1474314>
- Mesquita CS, Oliveira R, Bento F, Geraldo D, Rodrigues JV, Marcos JC (2014) Simplified 2, 4-dinitrophenylhydrazine spectrophotometric assay for quantification of carbonyls in oxidized proteins. *Anal Biochem* 458:69–71. <https://doi.org/10.1016/j.ab.2014.04.034>
- Mosmann T (1983) Rapid colorimetric assay for cellular growth and survival: application to proliferation and cytotoxicity assays. *J Immunol Methods* 65(1–2):55–63. [https://doi.org/10.1016/0022-1759\(83\)90303-4](https://doi.org/10.1016/0022-1759(83)90303-4)
- Mustachid D, Powis G (2000) Thioredoxin reductase. *Biochem J* 346(1):1–8
- Nag A, Verma P, Paul S, Kundu R (2022) In silico analysis of the apoptotic and HPV inhibitory roles of some selected phytochemicals detected from the rhizomes of greater cardamom. *Appl Biochem Biotechnol*. <https://doi.org/10.1007/s12010-022-04006-3>
- Pal A, Sengupta S, Kundu R (2021) *Tiliacora racemosa* leaves induce oxidative stress mediated DNA damage leading to G2/M phase arrest and apoptosis in cervical cancer cells SiHa. *J Ethnopharmacol* 269:113686. <https://doi.org/10.1016/j.jep.2020.113686>
- Paul S, Patra D, Kundu R (2019) Lignan enriched fraction (LRF) of *Phyllanthus amarus* promotes apoptotic cell death in human cervical cancer cells in vitro. *Sci Rep* 9(1):1–14. <https://doi.org/10.1038/s41598-019-51480-7>
- Perillo B, Di Donato M, Pezone A, Di Zazzo E, Giovannelli P, Galasso G, Castoria G, Migliaccio A (2020) ROS in cancer therapy: The bright side of the moon. *Exp Mol Med* 52(2):192–203. <https://doi.org/10.1038/s12276-020-0384-2>
- Pour LM, Farahnak A, Rad MM, Golmohamadi T, Eshraghian M (2014) Activity assay of glutathione S-transferase (GSTs) enzyme as a diagnostic biomarker for liver hydatid cyst in vitro. *Iran J Public Health* 43(7):994

- Singleton VL, Rossi JA (1965) Colorimetry of total phenolics with phosphomolybdic-phosphotungstic acid reagent. *Am J Enol Vitic* 16:144–158
- Su LJ, Zhang JH, Gomez H, Murugan R, Hong X, Xu D, Jiang F, Peng ZY (2019) Reactive oxygen species-induced lipid peroxidation in apoptosis, autophagy, and ferroptosis. *Oxidat Med Cell Longev*. <https://doi.org/10.1155/2019/5080843>
- Thomé MP, Filippi-Chiela EC, Villodre ES, Migliavaca CB, Onzi GR, Felipe KB, Lenz G (2016) Ratiometric analysis of Acridine Orange staining in the study of acidic organelles and autophagy. *J Cell Sci* 129(24):4622–4632. <https://doi.org/10.1242/jcs.195057>
- Townsend DM, Tew KD (2003) The role of glutathione-S-transferase in anti-cancer drug resistance. *Oncogene* 22(47):7369–7375. <https://doi.org/10.1038/sj.onc.1206940>
- Vernis L, El Banna N, Baille D, Hatem E, Heneman A, Huang ME (2017) Fe-S clusters emerging as targets of therapeutic drugs. *Oxidat Med Cell Longev*. <https://doi.org/10.1155/2017/3647657>
- Veskoukis AS, Margaritelis NV, Kyparos A, Paschalis V, Nikolaidis MG (2018) Spectrophotometric assays for measuring redox biomarkers in blood and tissues: the NADPH network. *Redox Rep* 23(1):47–56. <https://doi.org/10.1080/13510002.2017.1392695>
- Wang J, Mijiti Y, Chen Y, Liu Z (2021) Aryl hydrocarbon receptor is a prognostic biomarker and is correlated with immune responses in cervical cancer. *Bioengineered* 12(2):11922–11935. <https://doi.org/10.1080/21655979.2021.2006953>
- Wild R, Ooi L, Srikanth V, Münch G (2012) A quick, convenient and economical method for the reliable determination of methylglyoxal in millimolar concentrations: the N-acetyl-L-cysteine assay. *Anal Bioanal Chem Res* 403(9):2577–2581. <https://doi.org/10.1007/s00216-012-6086-4>
- Wu D, Yotnda P (2011) Production and detection of reactive oxygen species (ROS) in cancers. *JoVE (J Vis Exp)* 21(57):e3357. <https://doi.org/10.3791/3357>
- Yang Y, Chan WK (2021) Glycogen synthase kinase 3 beta regulates the human aryl hydrocarbon receptor cellular content and activity. *Int J Mol Sci* 22(11):6097. <https://doi.org/10.3390/ijms22116097>
- Ali SA, Khalil NY, Ahmed S, Rehmani FS, Yaqoob M and Yasinzai MM, (1998). Studies on the photometric estimation of citrate in urine. *Pak J Biol Sci*. 1998. <https://scialert.net/abstract/?doi=pjbs.1998.326.328>.
- Ervintari F, Puspitawati R, Utami S (2019) Effect of Curcuma Xanthorrhiza Roxb ethanol extract on the viability of Streptococcus mutans and Streptococcus sanguinis dual-species biofilms. *Int&nbsp;Pharm* <https://doi.org/10.22159/ijap.2019.v11s1.181>.
- Flohé L, Günzler WA (1984) Assays of glutathione peroxidase. In *Methods in enzymology* 105, 114–120. Academic Press. [https://doi.org/10.1016/s0076-6879\(84\)05015-1](https://doi.org/10.1016/s0076-6879(84)05015-1).
- Jiao Y, Wang Y, Guo S, Wang G (2017) Glutathione peroxidases as oncotargets. *Oncotarget*;8(45): 80093. <https://doi.org/10.18632/oncotarget.20278>.
- Sestili P, Calcabrini C, Diaz AR, Fimognari C, Stocchi V (2017) The fast-halo assay for the detection of DNA damage. In *Detection of DNA Damage (75–93)*. Humana Press, New York, NY. [https://doi.org/10.1007/978-1-4939-7187-9\\_6](https://doi.org/10.1007/978-1-4939-7187-9_6)
- Setyati WA, Subagiyo S, Pramesti R, Pringgenies D (2019) Effectiveness of herbal extract (Piper retrofractum, Curcuma aeruginosa, and Curcuma zanthorrhiza) as immunomodulator in non-specific immunity system of tiger grouper (Epinephelus fuscoguttatus) against infection from Vibrio alginolyticus and Vibrio parah. *Sci Technol Indones* 4(4):94–100. <https://doi.org/10.26554/sti.2019.4.4.94-100>.
- Sivanzade F, Bhalerao A, Cucullo L (2019). Analysis of the mitochondrial membrane potential using the cationic JC-1 dye as a sensitive fluorescent probe. *Bio-protoc*. 9(1):e3128 <https://doi.org/10.21769/BioProtoc.3128>
- Zhang X, Cheng X, Yu L, Yang J, Calvo R, Patnaik S, Hu X, Gao Q, Yang M, Lawas M, Delling M (2016) MCOLN1 is a ROS sensor in lysosomes that regulates autophagy *Nat&nbsp;Commun* 7(1), 1–12. <https://doi.org/10.1038/ncomms12109>.
- Rahmat E, Lee J, Kang Y (2021) Javanese turmeric (*Curcuma xanthorrhiza* Roxb.): ethnobotany, phytochemistry, biotechnology, and pharmacological activities. *Evid-Based Complement Altern Med* 2021:9960813
- Mehrotra R, Yadav K (2022) Cervical Cancer: formulation and implementation of Govt of India guidelines for screening and management. *Indian J Gynecol Oncol* 20(1):1–8. <https://doi.org/10.1007/s40944-021-00602-z>

Springer Nature or its licensor (e.g. a society or other partner) holds exclusive rights to this article under a publishing agreement with the author(s) or other rightsholder(s); author self-archiving of the accepted manuscript version of this article is solely governed by the terms of such publishing agreement and applicable law.